Title: Chemical inhibition of NAT10 corrects defects of laminopathic cells

Authors: Delphine Larrieu[1], Sébastien Britton[1,2], Mukerrem Demir[1],

Raphaël Rodriguez[3]* and Stephen P. Jackson*[1,4]

Affiliations:

[1]*The Wellcome Trust/Cancer Research UK Gurdon Institute and Department of Biochemistry, University of Cambridge, United Kingdom*

[2]*Current address: Université de Toulouse-Université Paul Sabatier, CNRS, Institut de Pharmacologie et de Biologie Structurale, Toulouse France*

[3]*Institut de Chimie des Substances Naturelles, CNRS, Gif-sur-Yvette, France*

[4]*The Wellcome Trust Sanger Institute, Hinxton, Cambridge, United Kingdom*

* Corresponding authors. Emails: s.jackson@gurdon.cam.ac.uk and raphael.rodriguez@cnrs.fr

One Sentence Summary: A new chemical strategy to correct nuclear architecture defects and improve fitness of laminopathic human cells.

Abstract: Downregulation and mutations of the nuclear-architecture proteins Lamin A and C cause misshapen nuclei and altered chromatin organization associated with cancer and laminopathies, including the premature-aging disease Hutchinson-Gilford progeria syndrome (HGPS). Here, we identified the small molecule "Remodelin" that improved nuclear architecture, chromatin organization and fitness of both human Lamin A/C depleted cells and HGPS-derived patient cells, and decreased markers of DNA damage in these cells. Using a combination of chemical, cellular and genetic approaches, we identified the acetyl-transferase protein NAT10 as the target of Remodelin that mediated nuclear shape rescue in laminopathic cells via microtubule reorganization. These findings provide insights into how NAT10 affects nuclear architecture, and suggest alternative strategies for treating laminopathies and aging.

Main Text:

Mutations in *LMNA,* which encodes Lamin A and C, cause pathologies known as laminopathies (*1*), including the accelerated-aging disease Hutchinson-Gilford progeria syndrome (HGPS) (*2, 3*). Deregulation of A-type lamins expression or localization also occurs in various cancers (*4-6*). Lamin A/C depletion or *LMNA* mutations cause enlarged, misshapen nuclei and altered chromatin organization (*7*). While some of these pathologies might reflect cell fragility, many likely result from downstream effects on chromatin structure, gene expression, DNA replication or DNA repair. Improving nuclear architecture of laminopathic cells can ameliorate defects in chromatin structure and other processes, thus improving some disease phenotypes (*8, 9*).

Lamin A/C depletion by small interfering RNA (siRNA) transfection (siLMNA) caused nuclear-shape defects (Fig. 1A, B, S1A, B), global chromatin relaxation and increased nuclear area (Fig. S1C, D). We therefore reasoned that modulating chromatin organization by lysine acetyltransferase (KAT) or lysine deacetylase (KDAC) inhibition might improve nuclear architecture defects of siLMNA cells. Compound screening identified the KAT inhibitor 4-(4-chlorophenyl)-2-(2-cyclopentylidenehydrazinyl)thiazole (**1**) (Fig. 1C) that restored nuclear circularity and global chromatin compaction in siLMNA cells (Fig. 1D, E, S1E-G). Although molecule **1** was identified in *Saccharomyces cerevisiae* as a GCN5 (General control of amino acid synthesis protein 5-like 2) network inhibitor (*10*), nuclear shape rescue was GCN5 independent, because the benchmark GCN5 inhibitor MB-3 had no effect on nuclear circularity. Complete nuclear-shape rescue occurred within 12 hours of treatment (Fig. 1F), independently of mitosis (Fig. S2A and Movie S1) and without markedly affecting the cell cycle (Fig. S2B, C). Moreover, compound **1** improved the nuclear morphology of several cancer cell lines displaying reduced

Lamin A/C expression (Fig. S2D, E), indicating that its effects were not specific to siRNA-mediated Lamin A/C depletion.

To identify putative targets of **1**, we synthesized a "clickable" cell-active analog **2** and used inactive molecule **3** as a negative control (Fig. 1G, H). We then employed "click-chemistry" to retrieve and validate drug-associated proteins. The alkyne "click" moiety selectively reacts with an azide group upon copper exposure, allowing tagging of the "clickable" molecules in cells (Fig. 1I). First, we used a biotinylated derivative of **2** (Fig. S3A), retrieved associated proteins with streptavidin beads, and identified several protein species whose staining intensities were reduced by an excess of competitor **1** (Fig. S2B). These proteins were then identified by mass spectrometry LC-MS/MS (Fig. S2C). N-acetyltransferase 10 (NAT10) was the only KAT protein identified, thus being the only likely relevant target of **1**. NAT10 was previously linked with the SUN1 nuclear envelope protein (*11*), whose depletion rescues nuclear shape in LMNA KO cells (*8*), and NAT10 KAT activity has been demonstrated towards microtubules and histones (*12*).

Pre-incubating clickable molecules with live cells followed by click pull-down identified NAT10 as a specific target of **2** in vivo (Fig. 1J), thereby establishing our protocol as a framework for identifying specific partners without photo-crosslinking agents (*13*). In parallel, we visualized sub-cellular localizations of clickable molecules by fluorescence microscopy (*14*) (Fig. 1K). This revealed that **2** specifically accumulated in nucleoli and also localized at the nuclear periphery and in the cytoplasm (Fig. 1K and Fig. S4A). Corroborating the binding studies, this distribution overlapped with that of NAT10, and moreover, NAT10 depletion (Fig. S4B) led to a marked reduction of molecule **2** in the nucleolus (Fig. 1K) without changes in nucleolar architecture (Fig.

S4C reveals that NAT10 localization was not affected by treatment with **1** or siLMNA). Furthermore, we established direct physical interaction between **1** and NAT10 using circular dichroism spectroscopy (Fig. S4D). Because molecule **1** was rapidly degraded upon light or air exposure, we explored its structural derivatives for their ability to rescue nuclear shape of siLMNA cells (Fig. S5A). The most potent and stable analog identified (**4;** Fig. S5B) was named "Remodelin" based on its ability to remodel nuclear architecture of siLMNA cells (Fig. 1L).

Consistent with a model in which Remodelin impacts on siLMNA cells through NAT10 targeting, we found that NAT10 depletion (Fig. 2A) corrected the aberrant nuclear morphology of siLMNA cells (Fig. 2B). Because **1**, the analog of Remodelin, is a KAT inhibitor, we assessed whether Remodelin affected NAT10 KAT activity. Aligning human NAT10 with the 3D structure of its bacterial homolog in complex with acetyl-CoA (*15*) led us to mutate conserved glycine-641 to glutamate (G641E), predicted to impair acetyl-CoA binding (Fig. 2C, D, S6A). Indeed, this mutation blocked NAT10 activity (Fig. 2E, S6B). Moreover, wild-type NAT10 activity was inhibited by Remodelin or clickable molecule **2**, establishing Remodelin as a bona fide NAT10 inhibitor. Complementation assays with siRNA-resistant wild-type (NAT10 WT) or G641E mutant NAT10 (NAT10 MUT) (Fig. S6C, D) showed that rescue of nuclear circularity in siLMNA cells required NAT10 catalytic function (Fig. 2F). Thus, inactivating NAT10 KAT activity by mutation or by Remodelin restores normal nuclear morphology in siLMNA cells.

We next investigated the effects of Remodelin on cells derived from *LMNA*-mutated HGPS patients (AG11498 and AG06297). HGPS cells accumulate Progerin, a permanently farnesylated, truncated form of Lamin A, leading to nuclear membrane folding and nuclear blebbing (Fig. 3A)

that contribute to the premature-aging phenotypes of HGPS patients. Remodelin significantly reduced the prevalence of misshapen nuclei in HGPS cells (Fig. 3B) as well as in primary MRC5 fibroblasts aged in culture (Fig. S7A, B), which also accumulate Progerin upon extended passaging (*16*). By contrast, Remodelin had no effect on non-laminopathic Werner syndrome cells (Fig. S7C, D). Farnesyltransferase inhibitors (FTIs) prevent accumulation of farnesylated Progerin at the nuclear membrane, thus reducing HGPS nuclear blebbing (*17*). Unlike FTIs, however, Remodelin did not trigger pre-Lamin A accumulation (Fig. S8A), indicating that Remodelin is not an FTI. Remodelin and FTI did not act synergistically on nuclear shape improvement, however, suggesting that they impact on a common pathway (Fig. S8B, C). Unlike Remodelin, FTI did not improve nuclear morphology in siLMNA cells. Furthermore, although FTI improves HGPS nuclear shape, it had the opposite effect on Progerin-negative cells, (Fig S8B, C) probably by causing accumulation of unprocessed Lamin A and B and centrosome separation defects (*18-20*). By contrast, Remodelin prevented FTI-induced nuclear shape defects in normal fibroblasts and U2OS cells (Fig. S8B-D). The proportion of misshapen nuclei in HGPS cells was similarly decreased by Remodelin treatment or NAT10 depletion (Fig. 3C and Fig. S9A), implying that NAT10 inhibition by Remodelin mediates nuclear shape normalization in HGPS cells.

While nuclear shape improvement is not always associated with overall amelioration of HGPS cell phenotypes (*21*), Remodelin improved global HGPS-cell fitness as observed by decreased steady-state levels of the DNA double-strand break markers γH2AX and autophosphorylated ATM, decreased DNA damage signaling (Fig. 3D, S9B-D), improved chromatin and nucleolar organization (assessed by histone H3K9me3 and NAT10 staining), and decreased SUN1 accumulation at the nuclear envelope (Fig. S9E-G). Blocking DNA damage signaling by inhibiting

the apical DNA-damage response kinases ATM and ATR decreased γH2AX (Fig. 3E, F). However, unlike Remodelin – which improved DNA replication (Fig. S9H), enhanced cell proliferation capacity (Fig. 3G) and decreased senescence (Fig. 3H; note other KAT inhibitors did not decrease senescence, Fig. S9I) – inhibiting ATM and ATR decreased proliferation and induced senescence (Fig. 3G, H). Similar effects were observed upon p53-pathway inhibition (Fig. S9I). Thus, Remodelin appears to reduce the amount of DNA damage in HGPS cells, while damage is still present but no longer signaled properly upon ATM/ATR inhibition, leading to cell growth arrest and senescence. Moreover, Remodelin conferred long-term benefits to HGPS cells, as seen by it decreasing senescence even after several weeks of treatment (Fig. 3I).

NAT10 localizes mainly in the nucleolus, which has a known role in maintaining nuclear shape (*22, 23*). For example, depleting the nucleolar protein NPM1 changes microtubule stability (*24*) and affects nuclear shape via connections between the cytoskeleton and nuclear envelope. Because tubulin is a known NAT10 substrate, we examined the microtubule network and observed network reorganization upon Remodelin treatment, NAT10 depletion, or mutational inactivation of NAT10 (Fig. 4A). In accord with there being a functional link between microtubule reorganization and nuclear shape rescue by NAT10 inhibition, the microtubule destabilizing drugs nocodazole and colchicine also rescued the nuclear shape defects of siLMNA cells (Fig. 4B) and HGPS cells (Fig. S10A), while latrunculin A, an actin polymerization inhibitor, increased nuclear distortion. Remodelin effects were not linked to Golgi apparatus fragmentation or tubulin depolymerization because, in contrast to nocodazole or colchicine, Remodelin did not affect Golgi apparatus integrity or tubulin polymer assembly (Fig. 4C and D), and did not cause cells to accumulate in mitosis.

To gain insight into how NAT10 modifies microtubule organization, we analysed microtubule regrowth dynamics. While initial microtubule regrowth (nucleation phase) appeared normal after NAT10 inhibition in siLMNA cells (Fig. 4E t=5 min) and HGPS cells (Fig. S10C), microtubule anchorage to centrosomes was affected by Remodelin in both siLMNA cells (Fig. 4E) and HGPS cells (Fig. S10B), or by the NAT10 G641E mutation (Fig. 4E t=15 min), indicating that NAT10 KAT activity promotes microtubule anchorage. These results suggest that inhibiting NAT10 KAT activity in laminopathic cells reduces microtubule anchorage, thereby releasing an external force on the nuclear envelope, thus contributing to nuclear shape rescue and global enhancement of cellular fitness (Fig. S11). This is in line with studies showing that releasing microtubule forces on the nucleus by growing them on a "soft" substrate normalizes the nuclear shape of laminopathic cells (*25*), and helps explain why Remodelin, like other microtubule reorganizing agents (*26*), corrects FTI-induced nuclear shape defects in non-progeric cells (Fig. S8).

Here, we have shown that the small molecule Remodelin improves nuclear shape and fitness of both progeric and Lamin A/C depleted cells via inhibiting NAT10. While these effects appear to be connected to NAT10 organizing the microtubule network, we cannot rule out that inhibiting additional nuclear functions of NAT10, related to chromatin, might also contribute to global improvement of cellular fitness. Small molecule inhibitors of NAT10 may thus provide additional ways to study laminopathy-associated processes with spatial and temporal resolution, as well as opportunities for alleviating dystrophic and premature-ageing diseases.

References and notes

1. H. J. Worman, G. Bonne, "Laminopathies": a wide spectrum of human diseases. *Exp Cell Res* **313**, 2121 (Jun 10, 2007).
2. A. De Sandre-Giovannoli *et al.*, Lamin a truncation in Hutchinson-Gilford progeria. *Science* **300**, 2055 (Jun 27, 2003).
3. M. Eriksson *et al.*, Recurrent de novo point mutations in lamin A cause Hutchinson-Gilford progeria syndrome. *Nature* **423**, 293 (May 15, 2003).
4. J. L. Broers *et al.*, Nuclear A-type lamins are differentially expressed in human lung cancer subtypes. *Am J Pathol* **143**, 211 (Jul, 1993).
5. S. F. Moss *et al.*, Decreased and aberrant nuclear lamin expression in gastrointestinal tract neoplasms. *Gut* **45**, 723 (Nov, 1999).
6. R. S. Venables *et al.*, Expression of individual lamins in basal cell carcinomas of the skin. *Br J Cancer* **84**, 512 (Feb, 2001).
7. G. Galiova, E. Bartova, I. Raska, J. Krejci, S. Kozubek, Chromatin changes induced by lamin A/C deficiency and the histone deacetylase inhibitor trichostatin A. *Eur J Cell Biol* **87**, 291 (May, 2008).
8. C. Y. Chen *et al.*, Accumulation of the inner nuclear envelope protein Sun1 is pathogenic in progeric and dystrophic laminopathies. *Cell* **149**, 565 (Apr 27, 2012).
9. J. I. Toth *et al.*, Blocking protein farnesyltransferase improves nuclear shape in fibroblasts from humans with progeroid syndromes. *Proc Natl Acad Sci U S A* **102**, 12873 (Sep 6, 2005).
10. F. Chimenti *et al.*, A novel histone acetyltransferase inhibitor modulating Gcn5 network: cyclopentylidene-[4-(4'-chlorophenyl)thiazol-2-yl)hydrazone. *J Med Chem* **52**, 530 (Jan 22, 2009).
11. Y. H. Chi, K. Haller, J. M. Peloponese, Jr., K. T. Jeang, Histone acetyltransferase hALP and nuclear membrane protein hsSUN1 function in de-condensation of mitotic chromosomes. *The Journal of biological chemistry* **282**, 27447 (Sep 14, 2007).
12. Q. Shen *et al.*, NAT10, a nucleolar protein, localizes to the midbody and regulates cytokinesis and acetylation of microtubules. *Exp Cell Res* **315**, 1653 (Jun 10, 2009).
13. S. E. Ong *et al.*, Identifying the proteins to which small-molecule probes and drugs bind in cells. *Proc Natl Acad Sci U S A* **106**, 4617 (Mar 24, 2009).
14. R. Rodriguez *et al.*, Small-molecule-induced DNA damage identifies alternative DNA structures in human genes. *Nat Chem Biol* **8**, 301 (Mar, 2012).
15. S. Chimnaronk *et al.*, RNA helicase module in an acetyltransferase that modifies a specific tRNA anticodon. *Embo J* **28**, 1362 (May 6, 2009).
16. P. Scaffidi, T. Misteli, Lamin A-dependent nuclear defects in human aging. *Science* **312**, 1059 (May 19, 2006).

17. B. C. Capell *et al.*, Inhibiting farnesylation of progerin prevents the characteristic nuclear blebbing of Hutchinson-Gilford progeria syndrome. *Proc Natl Acad Sci U S A* **102**, 12879 (Sep 6, 2005).

18. V. L. Verstraeten *et al.*, Protein farnesylation inhibitors cause donut-shaped cell nuclei attributable to a centrosome separation defect. *Proc Natl Acad Sci U S A* **108**, 4997 (Mar 22, 2011).

19. M. W. Glynn, T. W. Glover, Incomplete processing of mutant lamin A in Hutchinson-Gilford progeria leads to nuclear abnormalities, which are reversed by farnesyltransferase inhibition. *Hum Mol Genet* **14**, 2959 (Oct 15, 2005).

20. Y. Wang *et al.*, Blocking farnesylation of the prelamin A variant in Hutchinson-Gilford progeria syndrome alters the distribution of A-type lamins. *Nucleus* **3**, 452 (Sep-Oct, 2012).

21. M. X. Ibrahim *et al.*, Targeting isoprenylcysteine methylation ameliorates disease in a mouse model of progeria. *Science* **340**, 1330 (Jun 14, 2013).

22. M. A. Amin *et al.*, Fibrillarin, a nucleolar protein, is required for normal nuclear morphology and cellular growth in HeLa cells. *Biochem Biophys Res Commun* **360**, 320 (Aug 24, 2007).

23. M. A. Amin, S. Matsunaga, S. Uchiyama, K. Fukui, Depletion of nucleophosmin leads to distortion of nucleolar and nuclear structures in HeLa cells. *Biochem J* **415**, 345 (Nov 1, 2008).

24. G. Wang *et al.*, Nucleophosmin/B23 inhibits Eg5-mediated microtubule depolymerization by inactivating its ATPase activity. *The Journal of biological chemistry* **285**, 19060 (Jun 18, 2010).

25. C. Tamiello *et al.*, Soft substrates normalize nuclear morphology and prevent nuclear rupture in fibroblasts from a laminopathy patient with compound heterozygous LMNA mutations. *Nucleus* **4**, 61 (Jan-Feb, 2013).

26. N. Suzuki, K. Del Villar, F. Tamanoi, Farnesyltransferase inhibitors induce dramatic morphological changes of KNRK cells that are blocked by microtubule interfering agents. *Proc Natl Acad Sci U S A* **95**, 10499 (Sep 1, 1998).

Acknowledgements: We thank all members of the Jackson laboratory for help and support, J. Forment for discussions, K. Dry and J. Travers for discussions and critical reading of the manuscript. We thank Rimma Belotserkovskaya for the GFP-H2B U2OS cell line and Sonja Heidorn and Mathew Garnett (Wellcome Trust Sanger Institute) for providing us with the cancer cells used in the Lamin A/C expression screen. We thank Imagif and Institut de Chimie des Substances Naturelles, centre de recherche CNRS de Gif-sur-Yvette, France, for proteomic analysis. Research in the Jackson laboratory is funded by Cancer Research UK program grant

C6/A11224, the European Research Council, and the European Community Seventh Framework Programme grant agreement no. HEALTH-F2-2010-259893 (DDR). Core funding is provided by CRUK (C6946/A14492) and the Wellcome Trust (WT092096). S.P.J. receives his salary from the University of Cambridge, UK, supplemented by CRUK. D.L is funded by an EMBO Long-term fellowship ALTF 834-2011 and by a Project Grant from the Medical Research Council, UK MR/L019116/1, S.B. was funded by an EMBO Long-Term fellowship ALTF 93-2010 and Cancer Research UK. R.R. is supported by the Centre National de la Recherche Scientifique. M.D. is supported by the European Research Council grant DDREAM. The data in this publication form part of the subject matter of a patent application number 1405991.9.

Author Contributions. D.L. conceptualized the study and carried out all the experiments unless stated otherwise. S.B. cloned NAT10 expression constructs, performed the NAT10 structure analysis, produced high-resolution microscopy images and contributed to live cell imaging. R.R designed and synthesized the small molecules and performed circular dichroism spectroscopy experiment. R.R. and S.B. contributed equally to this work. M.D. provided assistance with IF, FACS and WB experiments. D.L. designed the experiments, analyzed the data and wrote the paper with contributions from SPJ, R.R. and S.B.

Supplementary Materials

Materials and Methods

Figs S1 to S11

Movie S1

Figures

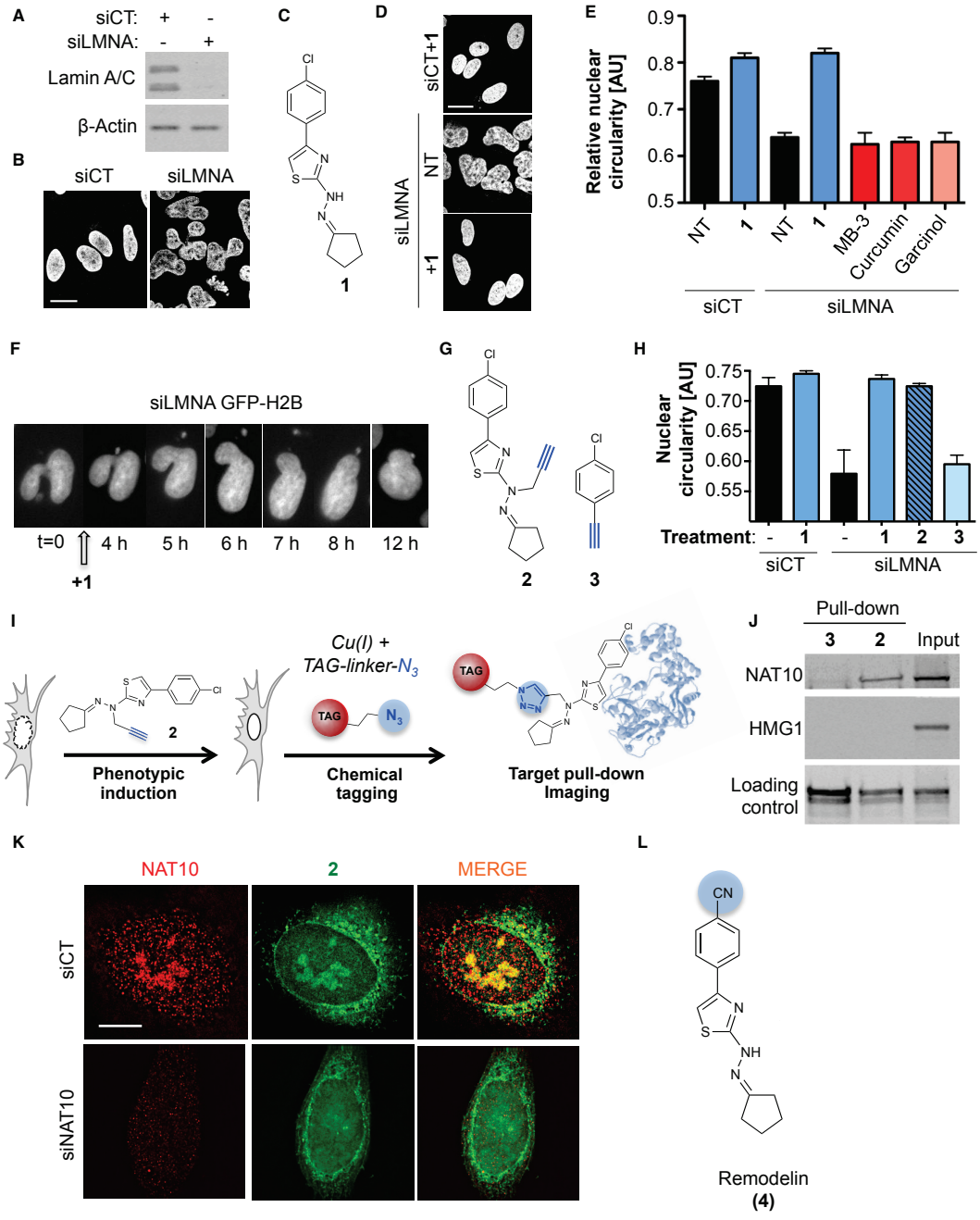

Figure 1: A small molecule restores nuclear shape in Lamin A/C depleted cells and targets the acetyltransferase NAT10. **A)** Lamin A/C depletion (siLMNA) in U2OS cells compared to negative control (siCT). **B)** Nuclear shape observed by DAPI staining. **C)** Molecular structure of

4-(4-chlorophenyl)-2-(2-cyclopentylidenehydrazinyl)thiazole **(1)**. **D)** Nuclear shape rescue observed by DAPI staining after treatment with **1**. **E)** Quantification of nuclear circularity in non-treated (NT) cells or cells treated with the indicated compounds (means of three independent experiments with n>212 ± s.d.). **F)** Live imaging pictures of nuclear shape rescue in GFP-H2B expressing U2OS cells transfected with siLMNA and treated with **1**. **G)** Molecular structure of clickable analogue **2** and clickable inactive control molecule **3**. **H)** Quantification of U2OS nuclear circularity (means of three independent experiments with n>224 ± s.d.) **I)** Principle of click-chemistry strategy for small molecule tagging. **J)** Pull-down of clickable molecules **2** and **3** pre-incubated in U2OS cells and analysis of bound proteins. **K)** Representative high-resolution microscopy pictures of NAT10 (red) and fluorescently labeled **2** (green) in control or NAT10 depleted cells (siNAT10). Scale bars: 10 μm. **L)** Molecular structure of Remodelin **(4)**, a stable and more potent analog of **1**.

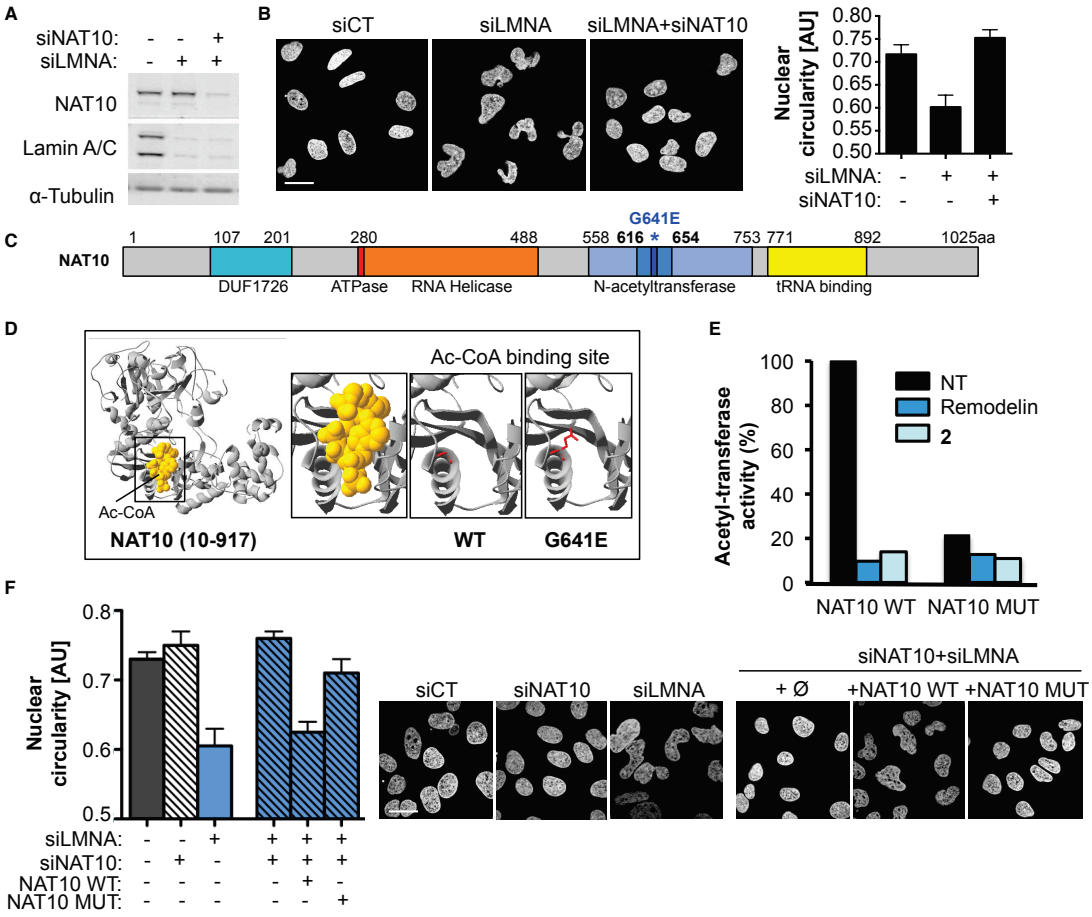

Figure 2: Inhibiting NAT10 activity by Remodelin mediates nuclear shape rescue of LMNA depleted cells. A) NAT10 and Lamin A/C depletion in U2OS cells. **B)** Nuclear shape visualized by DAPI staining (left) and quantification of nuclear circularity (right; means of three independent experiments with n>267 ± s.d.). Scale bar: 20 µm. **C)** Representation of NAT10 with its known domains. The G641E mutation identified in **D)** is indicated in dark blue and asterisked. **D)** Modelled 3D structure of human NAT10 residues 10-917 showing the acetyl-CoA binding site (left) and disruption of Ac-CoA binding by NAT10 G641E mutation (right) visualized with Swiss-Prot PDB Viewer. **E)** In vitro acetylation assay showing the activity of NAT10 towards tubulin. **F)** Quantification of nuclear circularity (left) in cells stably expressing siRNA-resistant FLAG-

NAT10 WT or FLAG-NAT10 G641E (NAT10 MUT; means of three independent experiments with n>198 ± s.d.) and nuclear shape visualized by DAPI staining (right). Scale bar: 20 μm.

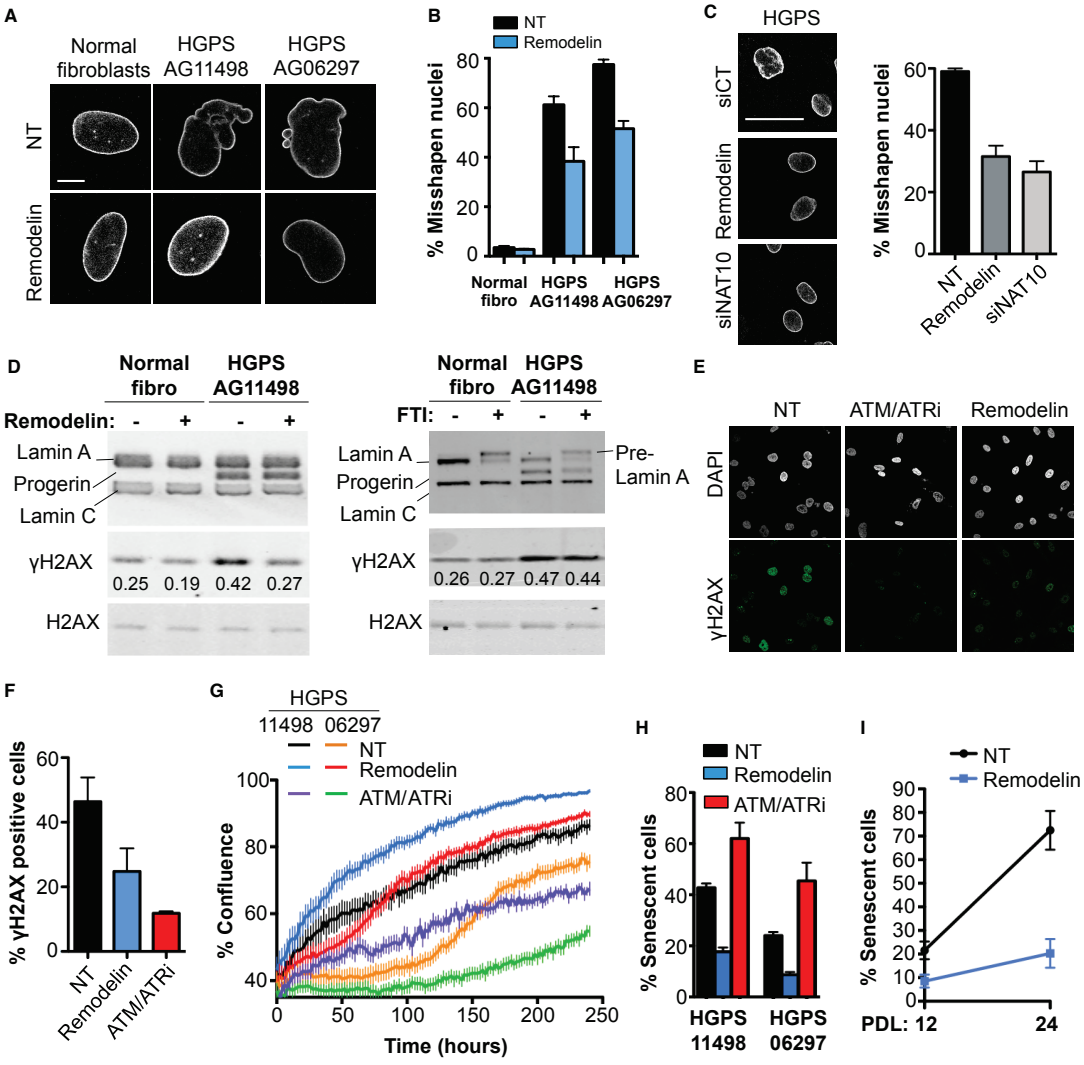

Figure 3: Remodelin targets NAT10 to improve nuclear shape and fitness of HGPS cells. A) Representative immunofluorescence (IF) pictures of Lamin A/C in HGPS cell lines compared to matched normal fibroblasts at the same population doubling. Scale bar: 10 µm. **B)** Quantification of misshapen nuclei upon Remodelin treatment (means of three independent experiments with n>213 ± s.e.m.). **C)** Lamin A/C staining in HGPS AG11498 cells (left) and quantification of misshapen nuclei (right; means of three independent experiments with n>176 ± s.e.m.). Scale bar: 50 µm. **D)** Western blotting analysis of γH2AX after Remodelin or FTI treatment. **E)**

Immunofluorescence analysis of γH2AX staining upon Remodelin or ATM/ATR inhibition (ATM/ATRi). **F)** Quantification of γH2AX positive cells observed by IF (means of three independent experiments with n>127 ± s.e.m.). **G)** HGPS proliferation upon Remodelin or ATM/ATR-inhibitor treatment (means of nine replicates ± s.e.m). **H)** Quantification of senescence-associated β-galactosidase positive cells (means of three independent experiments with n>257 ± s.e.m.). **I)** Quantification of senescence-associated β-galactosidase positive cells in HGPS AG11498 after 8 days of Remodelin treatment at population doubling 12 (PDL 12) and after several weeks of Remodelin treatment and 12 cell divisions (PDL 24) (means of two independent experiments with n>298 ± s.d.).

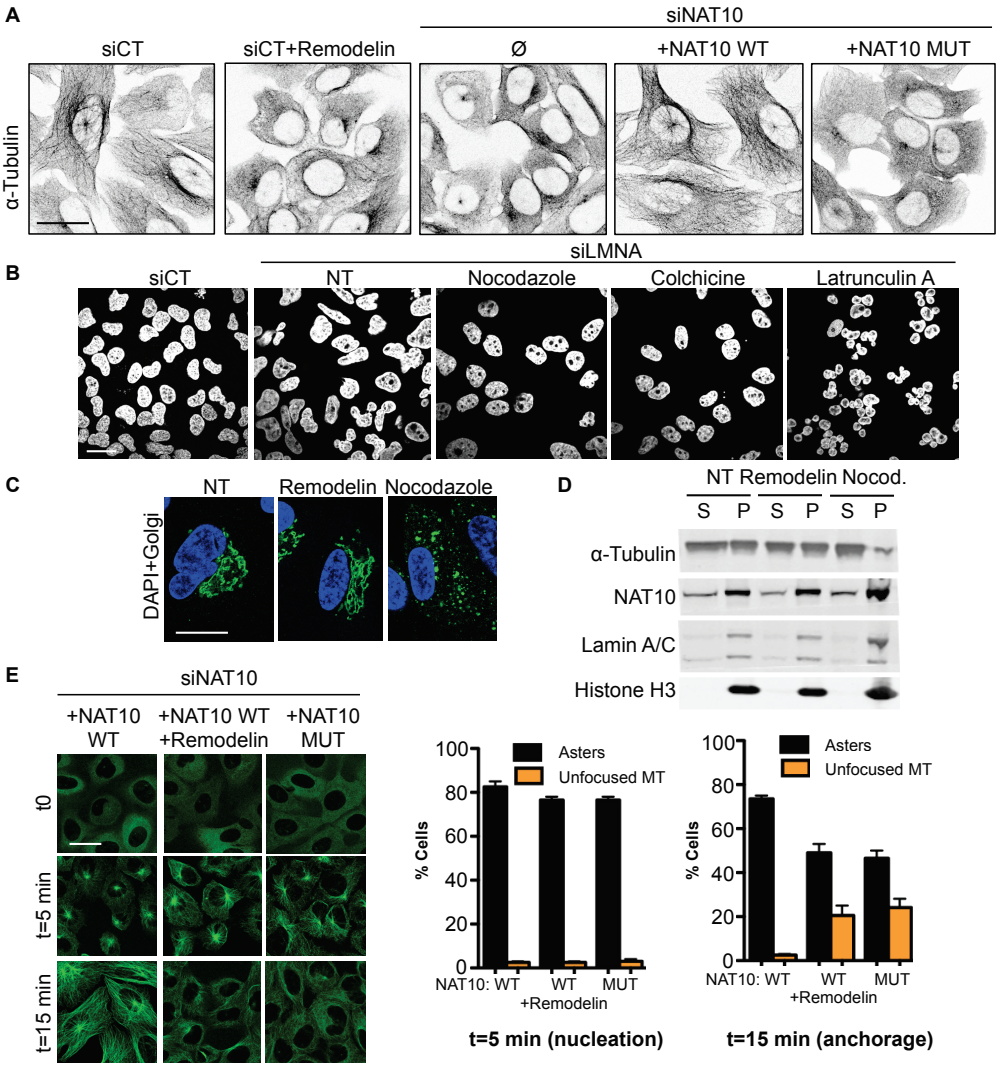

Figure 4: Inhibiting NAT10 acetyltransferase activity modifies microtubule organisation to rescue nuclear shape defects. A) Microtubule network visualisation by inverted IF pictures of α-tubulin. **B)** Nuclear shape visualisation after treating cells with microtubule or actin cytoskeleton disrupting agents. **C)** Visualisation of nuclear shape (DAPI, blue) and Golgi (anti-Giantin, green) integrity in siLMNA cells. **D)** Fractionation of polymerized (P) and soluble (S) tubulin upon Remodelin or nocodazole (Nocod.) treatment. **E)** Microtubule regrowth in cells transfected with siNAT10 and expressing the indicated siRNA-resistant constructs. α-tubulin IF staining (left)

shows nucleation phase: t=5 min and microtubule anchorage (t=15 min). Right: quantification of cells with indicated patterns (means of three independent experiments with n>103 ± s.e.m.).

Supplementary Materials for

Chemical inhibition of NAT10 corrects defects of laminopathic cells

Delphine Larrieu[1], Sébastien Britton[1,2], Mukerrem Demir[1], Raphaël Rodriguez[3]* and Stephen P. Jackson*[1,4]

* Corresponding authors.

Emails: s.jackson@gurdon.cam.ac.uk and raphael.rodriguez@cnrs.fr

This PDF file includes:

Materials and Methods
Figs. S1 to S11
Caption for Movie S1

Other Supplementary Materials for this manuscript includes the following:

Movie S1

Materials and Methods

Cell culture and transfections. U2OS and SaOS-2 osteosarcoma cells, HeLa cervical cancer cells, A431 melanoma cells, NCI-SNU5 gastric cancer cells, MRC-5 lung fibroblast cells and Werner syndrome patient-derived SV40 fibroblast cells were grown in Dulbecco's modified Eagle medium (DMEM, Sigma-Aldrich) supplemented with 10% fetal bovine serum (BioSera), 2mM L-glutamine, 100U per ml penicillin, 100 μg ml^{-1} streptomycin. Normal skin primary fibroblasts GM03440 and Hutchinson-Gilford progeria syndrome (HGPS) skin primary fibroblasts AG11498 and AG06297 were purchased from Coriell Cell Repositories and used between passage number 9-25. Cells were grown in DMEM supplemented as above. RPE-1 retinal pigment epithelial cells were grown in DMEM and Ham F12 mix medium supplemented as above and buffered with sodium bicarbonate. HMV-II melanoma cell line, 22RV1 prostate carcinoma cells, NCI-H82 and NCI-H69 lung carcinoma cells, and NCI-N87 gastric cancer cell lines were grown in RPMI-1640 medium (Sigma-Aldrich) supplemented as above. Stably transfected U2OS cells were maintained in standard medium containing 1mg ml^{-1} G418 (Invitrogen). siRNA duplexes were obtained from Life Sciences: Lamin A/C stealth RNAi: CCAUGAAGGAGGAACUGGACUUCCA and GCGUGAGGAGUUUAA-GGAGCUGAAA, NAT10 stealth RNAi: GAGCAUGGACCUCUCUGAAUACAUA, and as control siRNA, stealth RNAi negative control duplexes were used. Plasmid DNA and siRNA transfections were carried out using Lipofectamine 2000 and Lipofectamine RNAiMax (Life Sciences) respectively, following the manufacturer's instructions. Cells were analysed 48 to 72 h after transfection.

Drug treatments. The following KAT and KDAC inhibitors were included in the nuclear shape rescue screen, incubating cells with the molecules for 16 h: trichostatin A (1 μM), sodium butyrate (5 mM), tubacin (10 μM), SAHA (5 μM), curcumin (10 μM), garcinol (50 μM), anacardic acid (1 μM), MB-3 (5 μM), 4-(4-chlorophenyl)-2-(2-cyclopentylidenehydrazinyl)thiazole **(1)** (50 μM), 4-(4-chlorophenyl)-2-(2-cyclopentylidene-1-(prop-2-yn-1-yl)hydrazinyl)thiazole **(2)** (50 μM) and cyclopentylidene-[4-(4-cyanophenyl)thiazol-2-yl)hydrazine **(4)** (Remodelin) (10 to 50 μM). For HGPS cellular fitness assays, Remodelin was incubated at 1 μM for 1 to 10 days, renewing the medium every 3 days. For long-term senescence assay, cells were kept and passaged in medium containing 1 μM Remodelin or DMSO only for 12 population doublings. Senescence was assessed after 8 days of Remodelin treatment when cells were at Population Doubling 12, and then after several weeks of Remodelin treatment, when cells reached Population Doubling 24 using the Senescence β-Galactosidase Staining Kit #9860 from Cell Signaling. Nocodazole, colchicine and latrunculin A (Sigma-Aldrich) were used at 200ng/ml, 1 μg/ml and 1 μM respectively. Aphidicolin (Sigma-Aldrich) was used at 5 μg/ml for 16 h. Farnesyltransferase inhibitor FTI-277 was purchased from Tocris Bioscience and used at 5 μM. ATMi (KU55933) and ATRi (ATR-45) were obtained from Tocris Bioscience and from the Ohio State University respectively and used at 10 μM and 500 nM. Pifithrin alpha (Sigma-Aldrich) was used at 10 μM.

Live imaging of GFP-H2B cells. U2OS cells were transfected with siLMNA for 48h before addition of **(1)** at 50 μM. Pictures were acquired every 15 min for 16 h in z-stack of 0.2 μm interval with a Deltavision PersonalDV (Applied Precision, 512x512 CoolSNAP HQ2 camera) equipped with a 100x UPlanSApo/1.40 oil objective (Olympus) and controlled with SoftWoRx software (Applied Precision). Movies were then assembled from pictures with ImageJ software.

Flow cytometry. 10 μM EdU was incubated for 2 h when indicated. Cells were fixed in 4% paraformaldehyde (Sigma-Aldrich). EdU was fluorescently labeled using the Click-iT® EdU Flow Cytometry Assay Kit (Life Sciences). DNA was stained with 50 mg ml^{-1} propidium iodide (Sigma-Aldrich) in phosphate buffer solution (PBS) containing 0.1% Triton X-100 and 0.5mg ml^{-1} DNase free RNase A (Sigma-Aldrich). Samples were processed on a FACSCalibur flow cytometer equipped with CellQuest software (Becton Dickinson). Results were analysed by FlowJo software (TreeStar).

Nuclear circularity and nuclear area quantification. CellProfiler software was used to quantify nuclear circularity and nuclear area from DAPI staining pictures, using the "object size shape" measurement. The AreaShape measurement allowed the calculation of the Form Factor index ($4 \times \pi \times \text{Area}/\text{Perimeter}^2$) corresponding to circularity (a Form Factor of 1 reflecting a perfect circle), as well as the calculation of nuclear Area.

Proliferation assay. HGPS cells were plated at the same number in 24 well dishes. Next day, Remodelin (1 μM) or small molecule **1** (1 to 10 μM), were added to the wells and plates were transferred into an IncuCyte microscope (Essen BioScience). Phase contrast pictures were acquired every 2 h over 250 h. Percentage of cell confluence was calculated by the Cell Player integrated software (Essen BioScience) and analysed with GraphPad Prism® software.

Protein purification from human cells. HEK293 cells were transiently transfected with NAT10 constructs and harvested after 48 h in PBS. Cells were lysed for 5 min at room temperature in IP lysis buffer (20 mM Tris pH 7.5, 40 mM NaCl, 2 mM $MgCl_2$, 0.5% NP-40) freshly supplemented with 50 U/ml benzonase and EDTA-free protease inhibitor cocktail (Roche). After this initial lysis step, NaCl concentration was adjusted to 450 mM and samples were incubated at 4°C with rotation. Lysates were clarified by centrifugation (13,200 rpm, 20 min at 4°C), and after recovery NaCl concentration was equilibrated to 150 mM. Lysates were used for immunoprecipitation reaction in IP buffer (25 mM Tris pH 7.5, 150 mM NaCl, 1.5 mM DTT, 10% glycerol, 0.5% NP-40) supplemented with protease inhibitors. Target proteins were captured with anti FLAG antibody (Sigma-Aldrich) coupled to protein A/G-Dynabeads (Life Sciences). Complexes were washed with IP buffer containing incrementally increasing amounts of NaCl (250mM, 500mM, and 1M). Following this, the immuno-complexes were washed in TBS containing gradually decreasing amounts of NaCl (1M, 500mM, 250mM, and 150mM). At this point, elution was carried out using excess triple-Flag peptide (Sigma Aldrich). Eluted

proteins were loaded on a gel and the purification was verified by Silver Staining (SilverQuest kit, Life Sciences).

Analysis of soluble or polymerised tubulin. U2OS cells pre-treated with 5 μM Remodelin for 16 h or with 10 μM nocodazole for 8h, were lysed in MT Stabilization Buffer (MSB) (85 mM PIPES [pH 6.9], 1 mM EGTA, 1 mM $MgCl_2$, 2M glycerol, 0.5% Triton with 4 μg/ml Taxol). Lysates were kept at 4°C for 2 min and then centrifuged for 10 min at 13,000 rpm. Supernatants, representing the soluble fraction of proteins, were transferred to new tubes, and Laemmli buffer was added. Pellets, representing the polymerized fraction of proteins, were washed once in MSB without Triton, and then resuspended in Laemmli buffer. Equal amounts of lysate were loaded on a gradient gel.

Microtubules regrowth assay. 48 h after siRNA transfections, microtubules were depolymerized by cold treatment at 4°C for 1 h in cells pre-treated or not with 1 to 5 μM Remodelin for 16 h. Cold medium was replaced by pre-warmed medium and cells were incubated at 37°C for 5 or 15 min to allow microtubule nucleation and anchorage respectively. Cells were fixed in PFA and stained with anti α-Tubulin antibody as described in the immunofluorescence procedure.

Immunoblotting. Total cell extracts were prepared by scraping cells in SDS lysis buffer (4% SDS, 20% glycerol, and 120 mM Tris-HCl, pH 6.8), boiling for 5 min at 95°C, followed by 10 strokes through a 25-gauge needle. Before loading, lysates were diluted with a solution of 0.01% bromophenol blue and 200 mM DTT and boiled for 5 min at 95°C. Proteins were resolved by SDS-PAGE on 4-12% gradient gels (NUPAGE, Life Sciences) and transferred onto nitrocellulose membrane (Protran; Whatman). Secondary antibodies conjugated to IRDye 800CW were from LI-COR Biosciences. Detection and quantification was performed with an imager (Odyssey; LI-COR Biosciences).

Immunofluorescence. Cells were washed with PBS and fixed for 20 min with 2% PFA in PBS. Cells were permeabilised for 5 min with PBS/0.2% Triton X-100, and blocked with PBS/0.2% Tween 20 (PBS-T) containing 5% BSA. Coverslips were incubated for 1 h with primary antibodies and for 30 min with appropriate secondary antibodies coupled to Alexa Fluor 488 or 594 fluorophores (Life Technologies), before being incubated with 2μg/ml DAPI. Pictures were acquired with a FluoView 1000 confocal microscope (Olympus). For high resolution imaging, z-stacks were aquired with a Deltavision PersonalDV (Applied Precision, 1024x1024 CoolSNAP HQ2 camera, z-stack of 0.2 μm interval) or with a Deltavision OMX V3 in conventional mode (Applied Precision, 512x512 Cascade II cameras (Photometrics), z-stack of 0.125 μm interval) both equipped with a 100x UPlanSApo/1.40 oil objective (Olympus) and controlled with SoftWoRx software (Applied Precision). Deconvolutions were then performed with SoftWoRx (Applied Precision) in conservative mode. The different channels were acquired sequentially.

Fluorescent labeling of clickable molecules. Cells were pre-incubated with clickable molecules **2** or **3** for 2 h before being fixed and permeabilised as described above. Click reaction was prepared using Invitrogen Click-iT reagents with Alexa fluor 488 Azide and incubated with fixed cells for 1 h in the dark. In case of co-labeling with another protein, the click reaction was performed before the antibody incubations.

Antibodies. Antibodies used in this study are:

Abcam antibodies:	Santa Cruz antibodies:
Lamin A/C ab40567	Lamin A/C sc-6215
HMG1 ab18256	p53 (DO-1) sc-126
H2AX total ab11175	p21 sc-397
Histone H3 ab1791	
β-actin ab8226	Cell Signaling antibodies:
ATM (phospho S1981) ab81292	γH2AX 2577
SUN1 ab124770	p-Rb (Ser 807/811) 9308
anti-Giantin ab24586	Rb 9309
α-tubulin T9026	p-p53 (Ser15) 9284
H3K9me3 ab8898	
Sigma-Aldrich antibodies:	Others:
α-tubulin FITC F2168	γH2AX 05-636 Millipore
FLAG F3165	NAT10 13365-1-AP ProteinTech

Micrococcal nuclease digestion sensitivity assay. $1x10^6$ cells were trypsinized, harvested, and washed once with 1ml of 1xRSB buffer (10 mM Tris, pH 7.6, 15 mM NaCl, and 1.5 mM $MgCl_2$). After centrifugation (3,00 x g), the cell pellet was resuspended in 1 ml of 1x RSB buffer with 1% Triton-X 100 and homogenized by five strokes with a loose-fitting glass pestle to release nuclei. Nuclei were collected by centrifugation (13, 000 x g) and washed twice with 1 ml of buffer A (15 mM Tris, pH 7.5, 15 mM NaCl, 60 mM KCl, 0.34 M sucrose, 0.5 mM spermidine, 0.15 mM spermine, 0.25 mM PMSF, and 0.1% β-mercaptoethanol). Nuclei were resuspended in Buffer A and aliquoted into 100 µl aliquots. 1.2µl of 0.1 M CaCl2 was added to each aliquot and nuclei were digested by addition of 0.25 µl of 200 U/ml MNase (Sigma-Aldrich) and incubated at 30°C. Each aliquot was put back on ice at different time points and digestion was immediately stopped by addition of 3µl EDTA. DNA was purified using the Qiagen PCR purification kit and 1500 ng of DNA was analysed on a 1.5% agarose gel. Digestion profiles were analysed using ImageJ and values were adjusted relative to the global intensity of each lane to compensate for DNA loading variations.

Lysine acetyltransferase (KAT) assay. The KAT assay was performed using the Fluorescent HAT Assay kit (Active Motif) using NAT10 purified from HEK293 cells and 5 μg of purified MAP enriched Tubulin Porcine (Tebu-bio) as a substrate. Remodelin and clickable molecule **2** were used at 50 μM.

Circular Dichroism Spectroscopy. CD experiments were performed using a Chirascan Circular Dichroism Spectrophotometer (Applied Photophysics, UK). 200 μl of purified FLAG-NAT10 at a final concentration of 10 μM in TBS + 0.1 % NP-40 (Sigma-Aldrich) was placed in a quartz cuvette with an optical path length of 1 mm, transferred to the spectrophotometer. CD scans were recorded at 25°C over the wavelength range of 180 to 350 nm with a 1s response time, 1 nm pitch and 1.5-nm bandwidth. Compound **1** solubilized in DMSO was added and the solution was incubated for 5 min before recording scans. CD spectra were buffer subtracted, zero corrected at 300 nm and normalized (Molar ellipticity θ is quoted in 10^5 deg cm^2 $dmol^{-1}$).

DNA manipulations. All DNA constructs were validated to be mutation-free by DNA sequencing. A list of DNA oligonucleotides used in this study is provided below. pICE-FLAG was generated by cloning annealed primers FLAG-S and FLAG-AS into HindIII- and BamHI-digested pICE, a new synthetic plasmid conferring puromycin-resistance to mammalian cells (*29*). To generate NAT10 cDNA resistant to NAT10 siRNA, NAT10 cDNA was amplified from IMAGE clone 5166101 (Source Bioscience) using primer pairs NAT10-F and NAT10-siR-R, or NAT10-siR-F and NAT10-R. The resulting PCR products were fused together by PCR using primers NAT10-F and NAT10-R. The resulting PCR product was digested with BamHI and MluI and cloned into pICE-FLAG digested with the same restriction enzymes. To generate pICE-FLAG-NAT10-G641E, the G641E mutation was introduced into pICE-FLAG-NAT10 using QuickChange Site-Directed Mutagenesis kit (Agilent Technologies), according to the manufacturer's instructions and using primers NAT10-G641E-F and NAT10-G641E-R.

List of DNA oligonucleotides used in this study.

Name	**Sequence 5' to 3'**
FLAG-S	AGCTTGCGGCCGCCGCCACCATGGATTACAAGGATGACGACGATAAGG
FLAG-AS	GATCCCTTATCGTCGTCATCCTTGTAATCCATGGTGGCGGCGGCCGCA
NAT10-F	GCCGGATCCATGCATCGGAAAAAGGTGGATAACCG
NAT10-R	CGGACGCGTCTATTTCTTCCGCTTCAGTTTCATATC
NAT10-siR-F	CTGAAATCAATGGATTTGAGTGAATATATTATCCGTGGGGACGATGAAGAGTGG
NAT10-siR-R	GGATAATATATTCACTCAAATCCATTGATTTCAGCTTCCCTACTTCCTTCTTGTG
NAT10-G641E-F	CAAGGGATGGGCTATGAGAGCCGTGCTCTGCAG
NAT10-G641E-R	CTGCAGAGCACGGCTCTCATAGCCCATCCCTTG

Synthesis of Remodelin and derivatives. All solvents and reagents were purified using standard techniques or used as supplied from commercial sources (Sigma-Aldrich). NMR spectra were acquired on a Bruker 500 MHz instrument using deuterated solvents at 300 K. Notation for the ^{1}H NMR spectral splitting patterns includes: singlet (s), doublet (d), triplet (t), broad (br) and multiplet/overlapping peaks (m). Signals are quoted as □□values in ppm and coupling constants (J) are quoted in Hertz. Mass spectra were recorded on a Micromass® Q-Tof (ESI) spectrometer.

General procedure: The appropriate ketone or aldehyde was dissolved in isopropanol at a final concentration of 0.5 M and refluxed for 24h in the presence of an equimolar amount of thiosemicarbazide. The corresponding thiosemicarbazones were isolated by filtration and recrystallized from hot ethanol. Equimolar amounts of thiosemicarbazones and the desired haloketones were stirred at room temperature in isopropanol overnight at a final concentration of 0.2 M. The resulting products were recrystallized from hot ethanol several times to yield pure products and were used without further purification.

4-(4-chlorophenyl)-2-(2-cyclopentylidenehydrazinyl)thiazole hydrochloride salt (1)

Thiosemicarbazide (20 g, 220 mmol) and cyclopentanone (19.43 ml, 220 mmol) were refluxed in 500 ml of isopropanol for 24 h. The precipitate was filtered and recrystallized from hot ethanol to provide the corresponding thiosemicarbazone (2-cyclopentylidenehydrazine-1-carbothioamide) as pale yellow crystals. 2-cyclopentylidenehydrazine-1-carbothioamide (10 g, 63 mmol) and 2,4'-dichloroacetophenone (12 g, 63 mmol) were stirred overnight in 300 ml of isopropanol at room temperature. The precipitate was filtered and recrystallized from hot ethanol to yield the hydrochloride salt of the desired compound (16 g, 48 mmol, 77%) as light yellow needles. Spectral data were in agreement with those previously described in the literature (16). Molecule **1** was resuspended in DMSO at 10mg/ml.

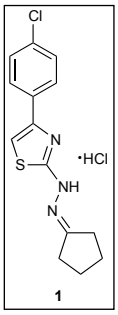

1

4-(4-chlorophenyl)-2-(2-cyclopentylidene-1-(prop-2-yn-1-yl)hydrazinyl)thiazole (2)

To a solution of **1** (1 g, 3 mmol) in freshly distilled DMF (75 ml) was added K_2CO_3 (1.375 g, 10 mmol), triethylamine (1.4 ml, 10 mmol) and propargyl bromide (1.2 ml, 5 mmol, 80 wt. % in toluene). The solution turned purple after 12 h at room temperature. Propargyl bromide (1.2 ml) was added and the reaction mixture was stirred for another 12 h. The solvent was then evaporated under reduced pressure and the crude residue dissolved in CH_2Cl_2, washed several times with saturated solutions of NH_4Cl and NaCl and dried over $MgSO_4$. The solvent was evaporated under reduced pressure and the desired product (0.35 g, 1 mmol, 34%) was obtained as a brown oil after regular column chromatography. TLC (Hexane : CH_2Cl_2, 80 : 20): R_f = 0.25; ^{1}H NMR (500 MHz, $CDCl_3$): δ 7.78 (d, J = 8.0 Hz, 2H), 7.32 (d, J = 8.0 Hz, 2H), 6.86 (s, 1H), 4.65 (s, 2H), 2.64–2.55 (m, 4H), 2.22 (s, 1H), 1.86–1.82 (m, 4H); ^{13}C NMR (125 MHz, $CDCl_3$): δ 184.9, 171.8, 150,6, 133.4, 133.3, 128.6 (2C), 127.3 (2C), 105.2, 78.3,

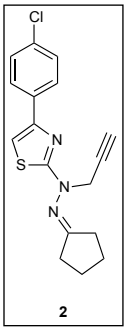

2

72.5, 42.7, 33.8, 31.5, 24.9, 24.4; HRMS (m/z): $[M]^+$ calcd. for $C_{17}H_{16}ClN_3S$, 329.0758; found, 329.0747. Molecule **2** was resuspended in DMSO at 10mg/ml.

1-Chloro-4-ethynilbenzene (Clickable inactive molecule **3**) was purchased from Sigma-Aldrich.

4-(4-cyanophenyl)-2-(2-cyclopentylidenehydrazinyl)thiazole (4, Remodelin)

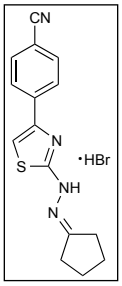

2-cyclopentylidenehydrazine-1-carbothioamide (1 g, 4.46 mmol) and 2-bromo-4'-cyanoacetophenone (700 mg, 4.45 mmol) were stirred overnight in 12 ml of isopropanol at room temperature. The precipitate was filtered and recrystallized from hot ethanol to yield the hydrobromide salt of the desired compound (559 mg, 1.98 mmol, 45%) as light yellow needles. ^{1}H NMR (500 MHz, $CDCl_3$): δ 12.11 (br s), 7.84 (d, J = 9.0 Hz, 2H), 7.81 (d, J = 9.0 Hz, 2H), 6.84 (s, 1H), 2.61 (t, J = 9.0 Hz, 2H), 2.51 (t, J = 9.0 Hz, 2H), 1.94–1.80 (m, 4H); ^{13}C NMR (125 MHz, $CDCl_3$): δ 173.8, 169.5, 138.8, 133.5, 131.3, 126.3, 118.0, 114.1, 103.8, 33.7, 31.2, 25.2, 25.0; HRMS (m/z): $[M]^+$ calcd. for $C_{15}H_{15}N_4S$, 283.1009; found, 283.1017. Molecule **4** was resuspended in DMSO at 10mg/ml.

Small molecules for protein pull-down assays. Biotinylated derivative **5** was synthesized from compounds **2**, commercially available O-(2-aminoethyl)-O'-(2-azidoethyl)heptaethylene glycol and (+)-biotin N-hydroxysuccinimide. Biotinylated derivatives **6** and control **7** were generated *in situ* from **2** and **3**, by addition of PEG4 carboxamide-6-azidohexanyl biotin (Life Sciences) and click reagents in cell extracts.

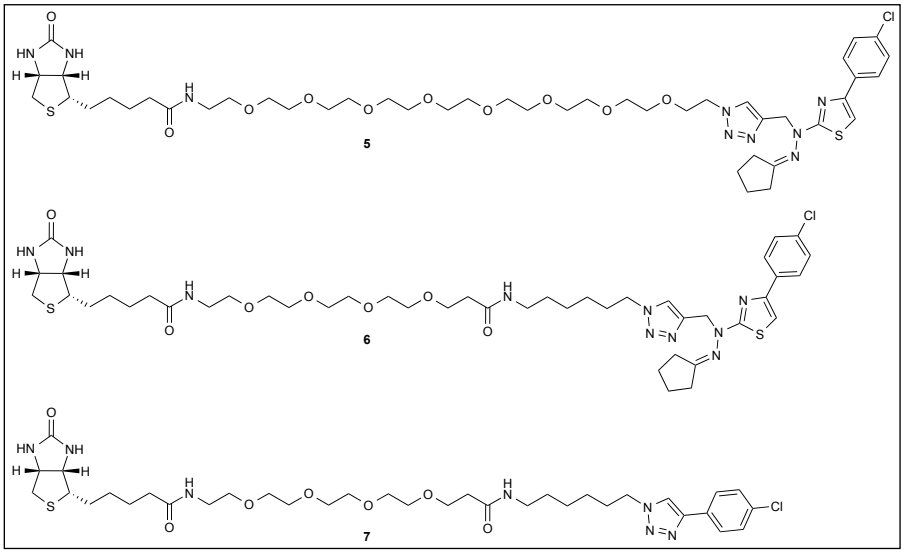

Biotinylated small molecule pull-downs. Cells were harvested in PBS and lysed in RIPA buffer supplemented with 1 mM PMSF and protease inhibitors (Roche) for 30 min at 4°C with rotation. The supernatants were collected by centrifugation at 16,000 x g for 10 min. Supernatants were then incubated with 40 μM of biotinylated small molecule or

for the competition experiment with 200 μM of **(1)** and 40 μM of biotinylated compound for 2 h. Streptavidin coated magnetic beads (Dynabeads M-280 Streptavidin, Life Sciences) were washed 3 times with binding buffer (25 mM Tris.HCl, 150 mM NaCl, 0.1% Triton) and incubated with supernatants for 1 h at 4°C with rotation. The magnetic beads were washed 3 times with the binding buffer followed by boiling in Laemmli buffer for 5 min to elute the proteins. Samples were then loaded on 4-12% gradient gels (NUPAGE, Life Sciences), analyzed by silver staining (SilverQuest staining kit, Life Sciences) and specific bands were cut and analysed by LC-MS/MS.

Clickable small molecule pull-downs. Cells were incubated with clickable compounds **2** and control **3** for 2 h and cell lysates were prepared as described above. Small molecules were then coupled to biotin using the click reaction to form molecules **6** and **7**. Click reaction reagents were added to the cell lysates as follows: 10 μM biotin azide (PEG4 carboxamide-6-Azidohexanyl Biotin, Life Sciences), 10 mM sodium ascorbate (Sigma-Aldrich), 2 mM $CuSO_4$ (Life Sciences). Click reactions were incubated in the dark for 1 h at 4°C with rotation. Streptavidin beads were then incubated for 1 h and samples were eluted and loaded on a gel as described above, before immunoblotting.

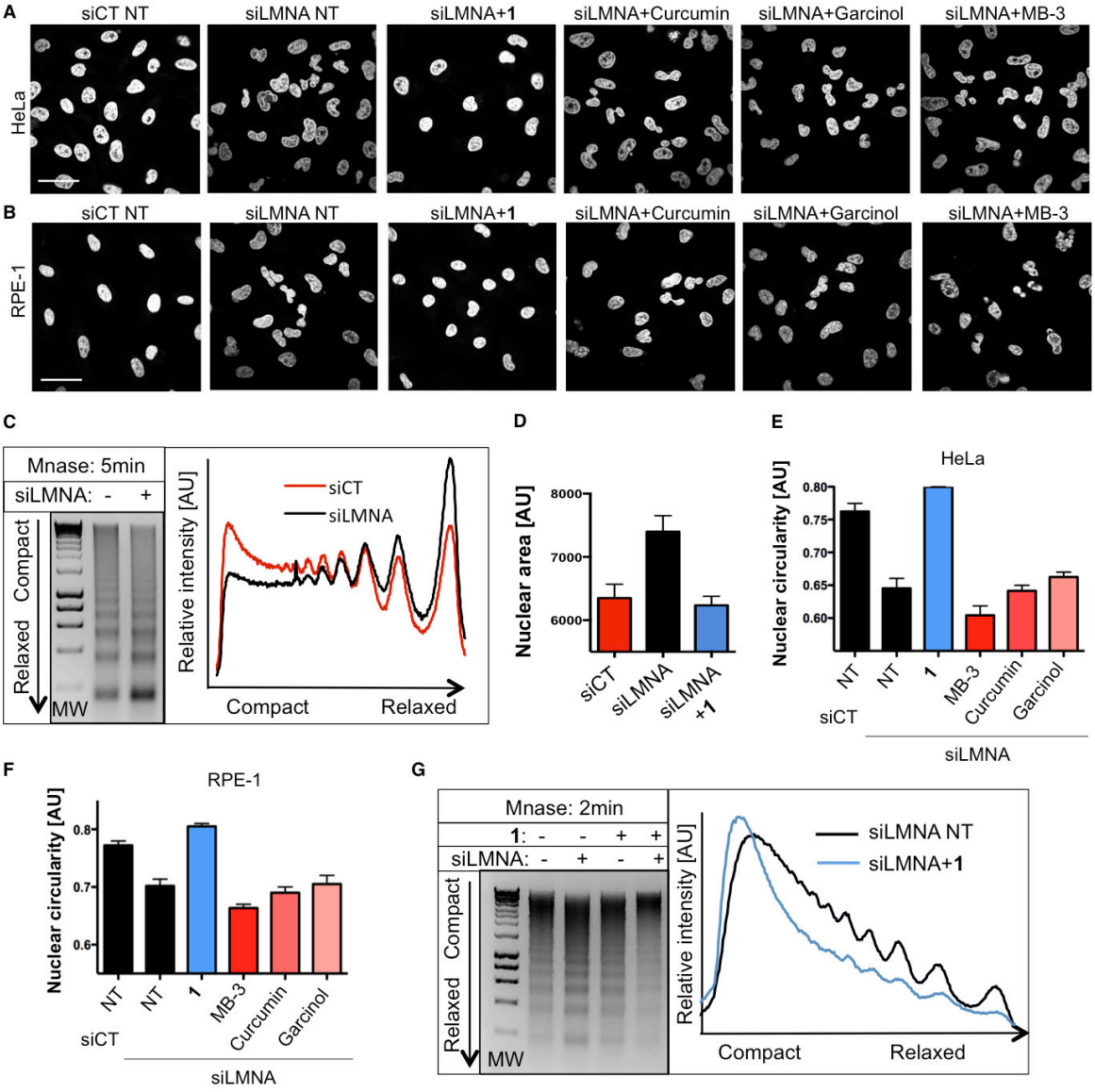

Fig. S1: Small molecule 1 rescues nuclear shape defects and chromatin compaction of Lamin A/C depleted cells. A) and **B)** Nuclear shape visualization by DAPI staining of HeLa **(A)** or RPE-1 **(B)** cells depleted for Lamin A/C (siLMNA) and treated with various KAT inhibitors. Scale bars: 50 µm. **C)** Representative MNase digestion profile (left) in U2OS cells from three independent experiments and corresponding quantification (right). **D)** Quantification of nuclear area in U2OS cells (means of three independent experiments with n>198± s.d.). **E)** and **F)** Cell Profiler quantification of nuclear circularity of HeLa **(E)** or RPE-1 **(F)** cells from DAPI staining as shown in **A)** and **B)** (means of three independent experiments with n>252 ± s.d). **G)** Representative MNase digestion profile in U2OS cells (left) from three independent experiments and corresponding quantification of siLMNA cells (right).

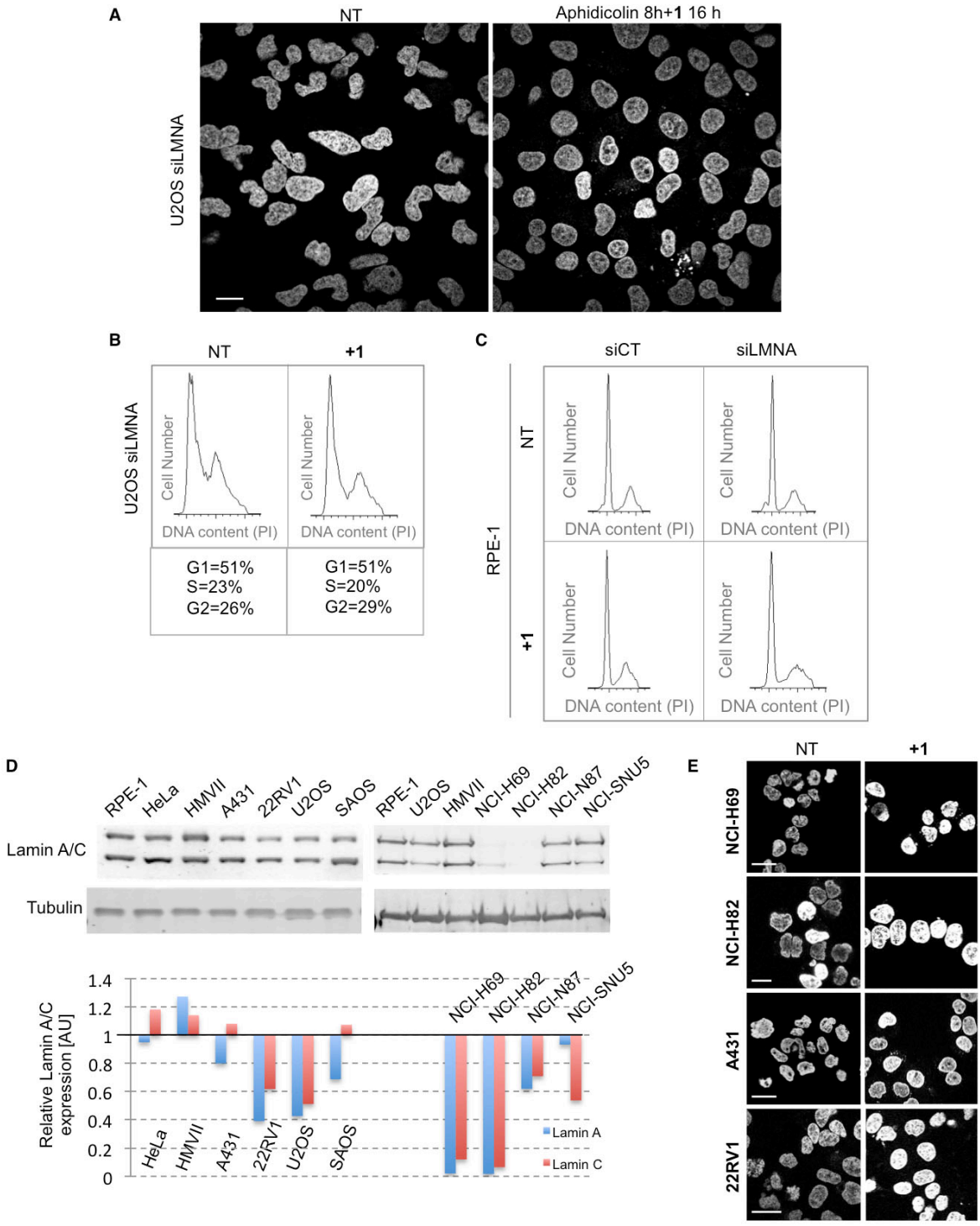

Fig. S2: Small molecule 1 acts independently of the cell cycle and improves nuclear shape in cancer cells with low Lamin A/C expression. A) Nuclear shape rescue of LMNA depleted cells after treatment with **1** is independent of mitosis, and still occurs in cells synchronized in S phase by aphidicolin to prevent mitotic entry. Scale bars: 20 µm. **B)** and **C)** Cell cycle profiles of indicated cell lines analysed by flow cytometry. PI: propidium iodide. Scale bars: 20 µm. **D)** Analysis of Lamin A/C expression levels in

indicated cancer cell lines. Bottom panel: Image J quantification of Lamin A/C expression in cancer cells relative to normal RPE-1 cells. **E)** Representative pictures of DAPI staining showing nuclear shape improvement in low Lamin A/C expressing cancer cells after treatment with **1**. Scale bars: 20 μm.

A

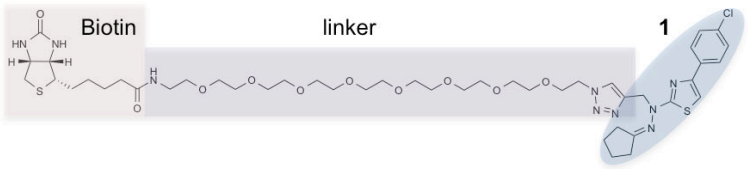

B

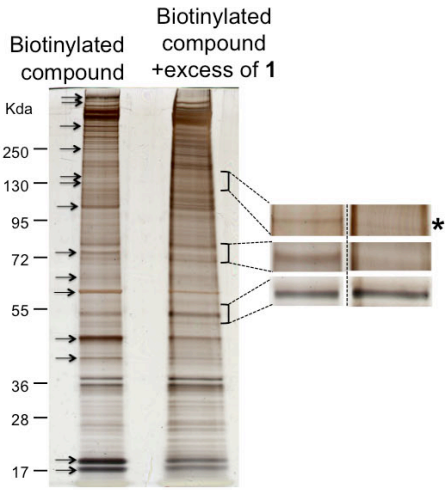

C

RNA/nucleolus	peptide hits	protein name
Q3SZ63	2	Nucleolar protein 56
A4FUD3	3	116 kDa U5 small nuclear ribonucleoprotein component
Q1HR24	3	40S ribosomal protein S14
Q76I82	3	40S ribosomal protein S15a
Q3T0X6	3	40S ribosomal protein S16
Q6Q311	3	40S ribosomal protein S25
Q4R5I3	2	60S ribosomal protein L22
Q3T057	3	60S ribosomal protein L23
Q3T0D5	2	60S ribosomal protein L30
Q3T171	3	60S ribosomal protein L36
Q02878	5	60S ribosomal protein L6
Q99020	2	Heterogeneous nuclear ribonucleoprotein A/B
A5A6H4	3	Heterogeneous nuclear ribonucleoprotein A1
Q6URK4	5	Heterogeneous nuclear ribonucleoprotein A3
Q5RA82	2	Heterogeneous nuclear ribonucleoprotein C
Q14103	3	Heterogeneous nuclear ribonucleoprotein D0
Q4R4M6	6	Heterogeneous nuclear ribonucleoprotein K
Q8VEK3	8	Heterogeneous nuclear ribonucleoprotein U
Q2HJ60	8	Heterogeneous nuclear ribonucleoproteins A2/B1
Q9H0A0	**8**	**N-acetyltransferase 10 (NAT10)**
Q9NR30	5	Nucleolar RNA helicase 2
Q3T160	2	Nucleophosmin
Q08E38	2	Pre-mRNA-processing factor 19
A1A5S1	3	Pre-mRNA-processing factor 6
Q5RAS1	3	pre-rRNA processing protein FTSJ3
Q4R6M5	16	Probable ATP-dependent RNA helicase DDX5
Q9D903	2	Probable rRNA-processing protein EBP2
Q28009	5	RNA-binding protein FUS
Q9UKM9	8	RNA-binding protein Raly
O75691	41	Small subunit processome component 20 homolog

Nuclear envelope	peptide hits	protein name
Q5SRE5	4	Nucleoporin NUP188 homolog
P20700	5	Lamin-B1
Q03252	22	Lamin-B2

Chromatin	peptide hits	protein name
Q91ZW3	2	SMARCA5
Q9QZQ8	3	Core histone macro-H2A.1
Q8CCK0	2	Core histone macro-H2A.2
Q6URC2	3	High mobility group protein HMG-I/HMG-Y
P0C0S8	3	Histone H2A type 1
A9UMV8	3	Histone H2A.J
P02272	3	Histone H2A.V
Q2M2T1	4	Histone H2B type 1-K
P18437	2	Non-histone chromosomal protein HMG-17

Cytoskeleton	peptide hits	protein name
A2BDB0	21	Gamma-actin
P15924	2	Desmoplakin
P21333	8	Filamin-A
Q14315	7	Filamin-C
P35527	6	Keratin, type I
Q5R844	3	Myosin light polypeptide 6
P48681	2	Nestin
A6QQJ3	2	Peripherin
Q15149	46	Plectin
O94915	4	Protein furry homolog-like
Q54HF0	4	Putative actin-25
Q9NYL9	3	Tropomodulin-3
P23729	2	Type III intermediate filament
O43795	15	Unconventional myosin-Ib
O00159	21	Unconventional myosin-Ic
O94832	3	Unconventional myosin-Id
P08670	52	Vimentin

Trafficking	peptide hits	protein name
Q6P5F9	4	Exportin-1
Q9EPL8	2	Importin-7

	peptide hits	protein name
P46940	2	Ras GTPase-activating-like protein IQGAP1
Q86VI3	4	Ras GTPase-activating-like protein IQGAP3

Fig. S3: Biotin analog of 1 retrieves the acetyl-transferase protein NAT10. A) Molecular structure of biotinylated analogue. **B)** Silver staining of proteins after pull-down of biotinylated molecule and identification of specific bands (see arrows) decreasing in the presence of 5 equivalents of non-clickable molecule **1**. The band

corresponding to NAT10 is magnified on the right (*) together with other specific and non-specific bands. **C)** Specific protein hits retrieved by biotinylated small molecule and identified by liquid chromatography-tandem mass spectrometry (LC-MS/MS).

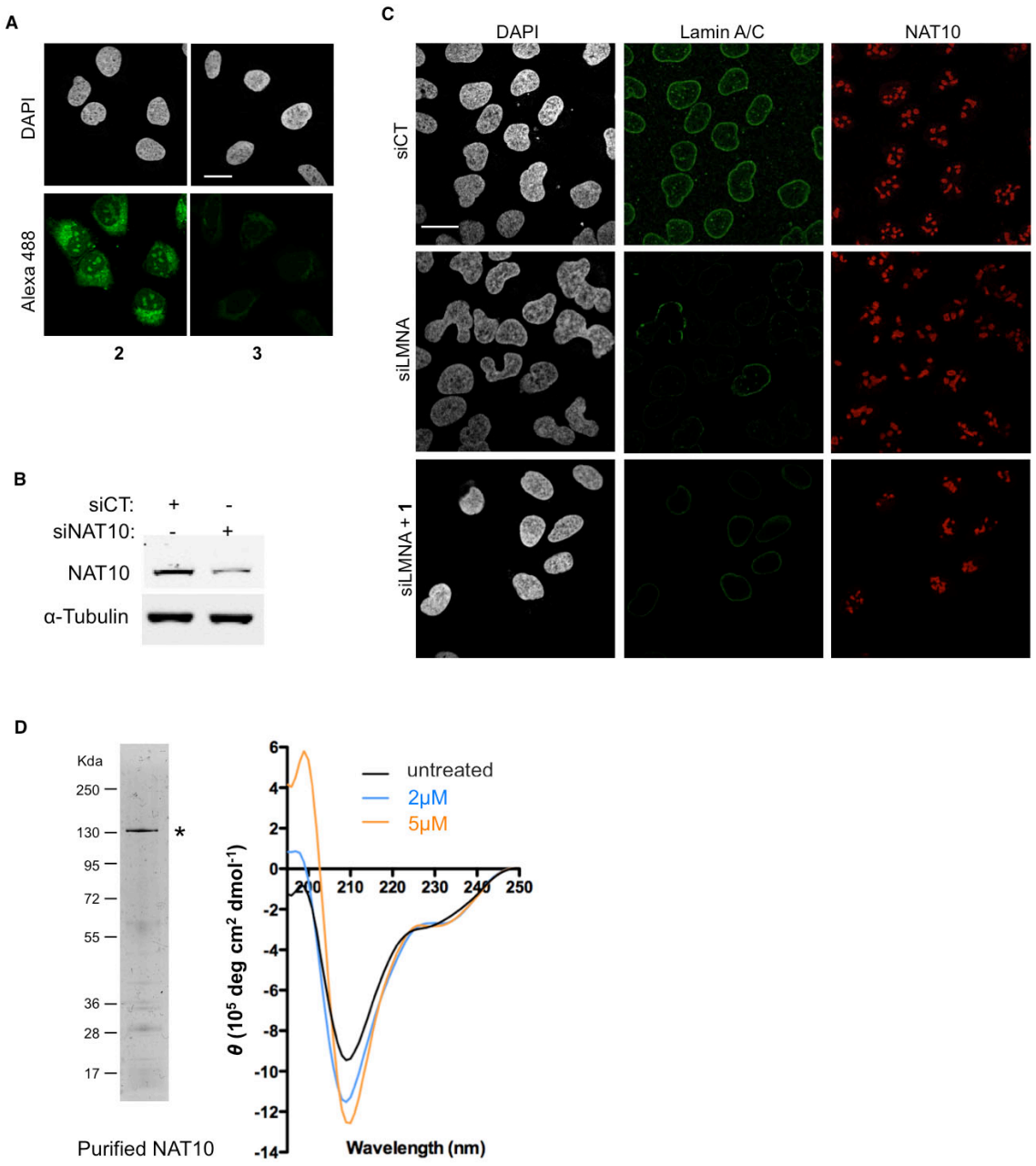

Fig. S4: Subcellular localization of the molecules and analysis of Remodelin binding to purified NAT10. A) Fluorescent labeling of clickable control molecule **3** showing no specific staining, contrasting to molecule **2** (see Fig. 1K). Scale bar: 20 µm. **B)** NAT10 depletion by siRNA (siNAT10) is observed by western blotting. **C)** IF pictures of Lamin A/C and NAT10 staining within cells transfected or treated as indicated. Scale bar: 20 µm. **D)** NAT10 was expressed and purified in human HEK293 cells and analysed by silver staining (left *). NAT10 folding was assessed by circular dichroism spectroscopy (right). In the absence of compound, the NAT10 spectra displayed a characteristic negative signal at 210 nm, reflecting the presence of α-helices. Upon addition of

molecule **1**, absolute molar ellipticity increased, consistent with stabilization of NAT10 by supramolecular stapling (*30*) and suggesting that stabilization of protein folding by **1** might inhibit NAT10 activity.

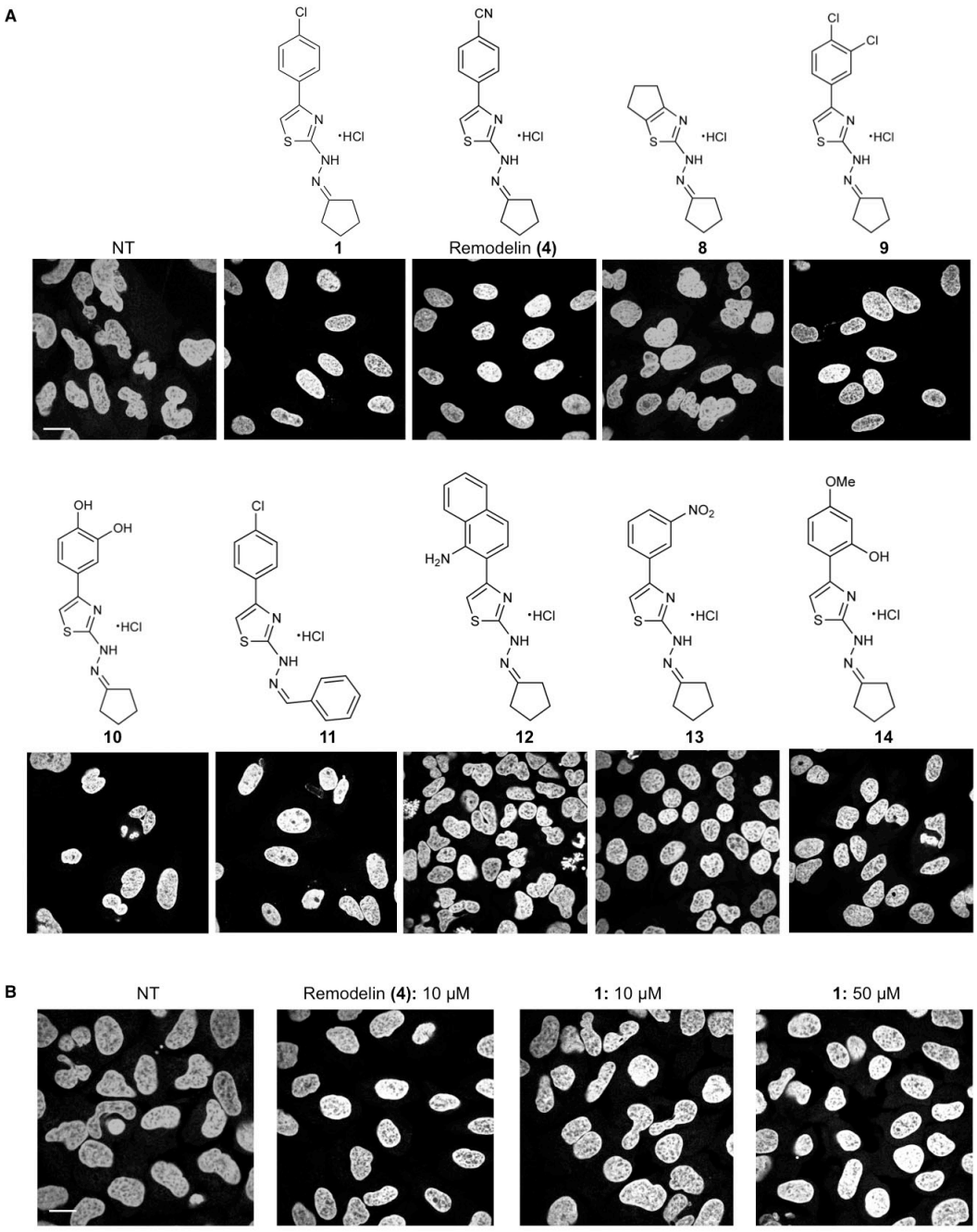

Fig. S5: Screening of 1 analogs to identify structural requirements for nuclear shape rescue. A) Nuclear shape analysis by DAPI staining in siLMNA cells treated with the indicated analogs of **1**. **B)** Dose-dependent nuclear shape rescue observed by DAPI staining of siLMNA cells, showing an ~5-fold increase in the potency of Remodelin compared to **1**. Scale bar: 20 μm.

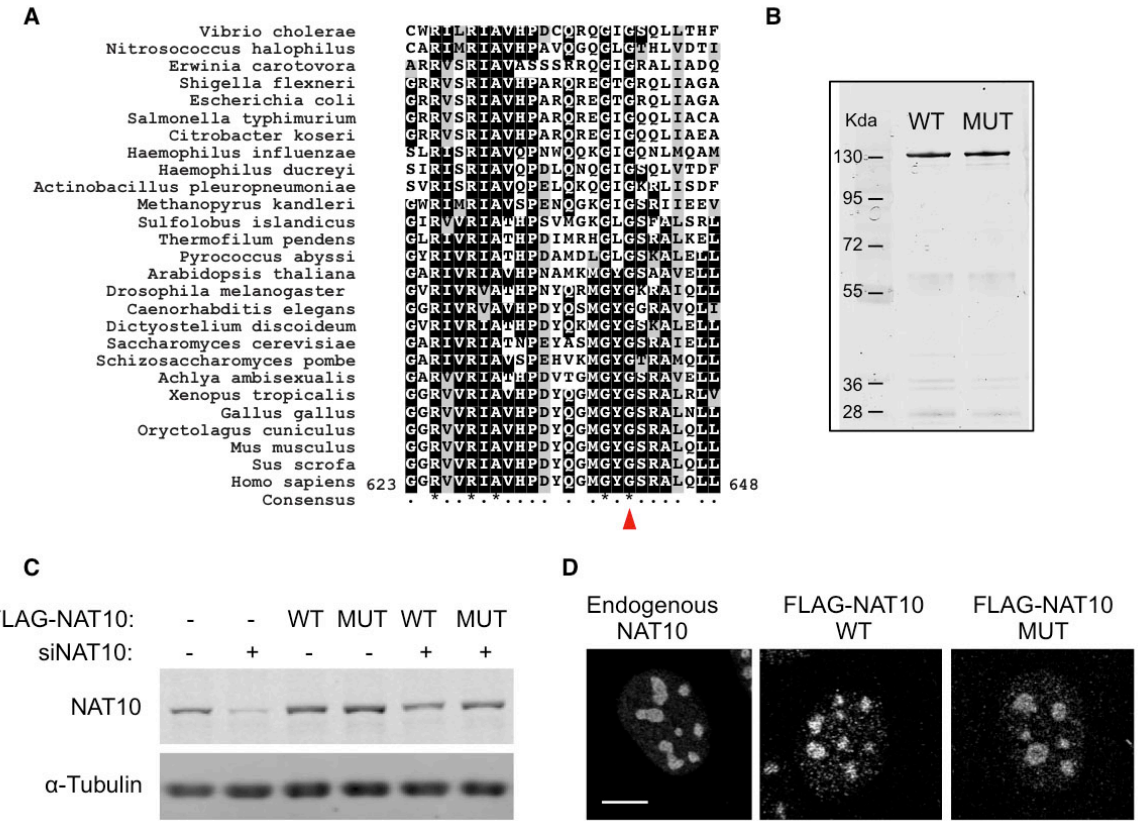

Fig. S6: NAT10 mutation G641E (MUT) does not affect its localization. A) Alignment of NAT10 GNAT (Gcn5-related N-acetyltransferase) domain showing the conservation of G641. **B)** Silver staining of purified FLAG-NAT10 WT or G641E mutant (MUT) from Human HEK293 cells. These proteins were used in acetyl-transferase activity assays (Fig. 2E). **C)** Characterization of U2OS cells stably expressing siRNA resistant constructs of FLAG-NAT10 WT and MUT. Expression of constructs and siRNA resistance was assessed by western blotting and **D)** the correct localization of both constructs was verified by IF staining using anti-NAT10 antibody or anti-FLAG antibody. Scale bars: 10 µm.

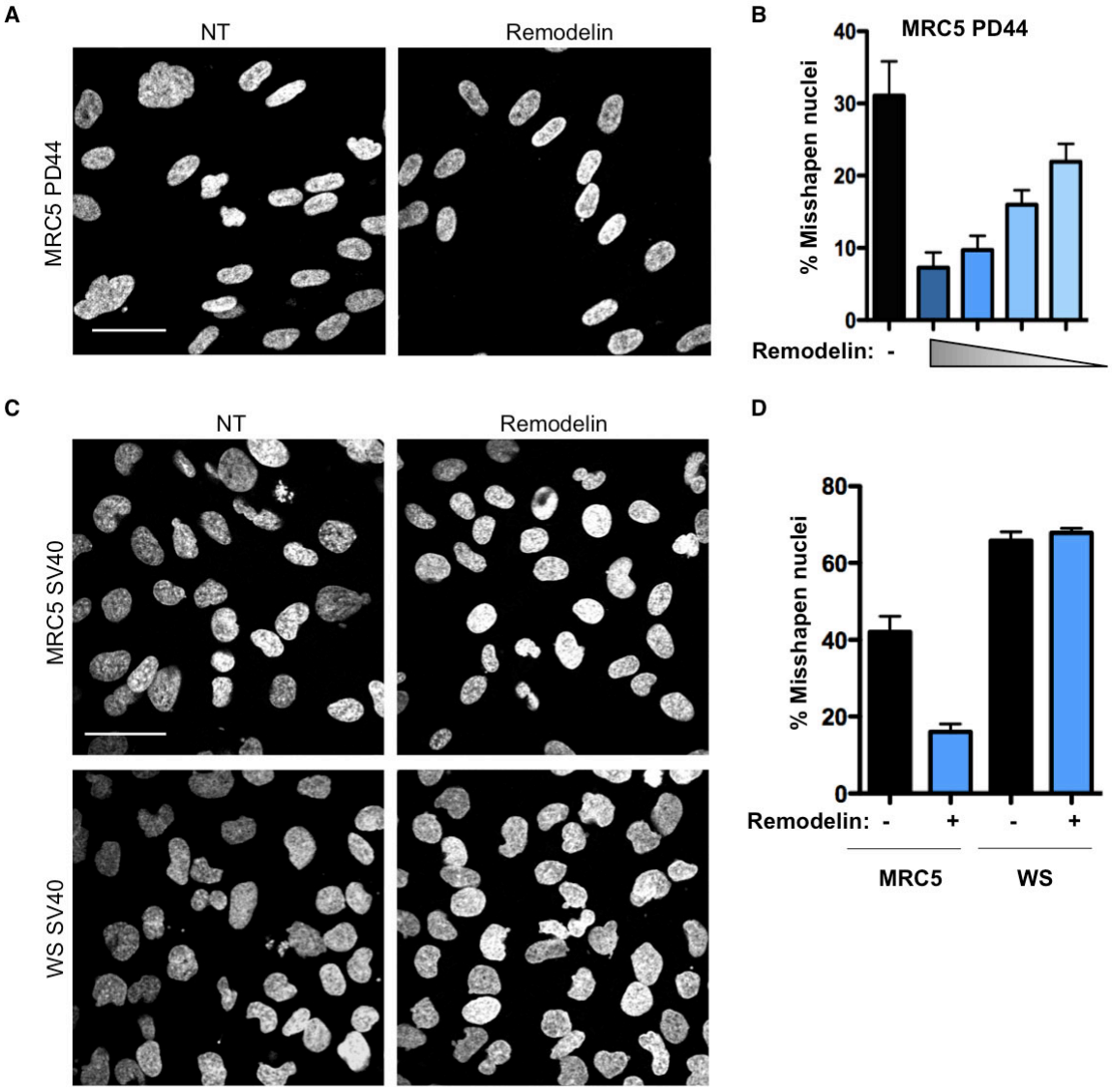

Fig. S7: Remodelin rescues nuclear shape of aged MRC5 cells but not Werner Syndrome cells in a dose-dependent manner. A) Misshapen nuclei observed by DAPI staining in MRC5 aged cells in culture, at population doubling 44 (PD44) was rescued by Remodelin. B) Quantification of misshapen nuclei after increasing concentrations of Remodelin (mean of three independent experiments ± s.e.m.). C) DAPI staining of non-laminopathic Werner syndrome cells showing no nuclear shape improvement upon Remodelin treatment. D) Cell Profiler quantification of misshapen nuclei (means of three independent experiments ± s.d. n>273). Scale bars: 50 μm.

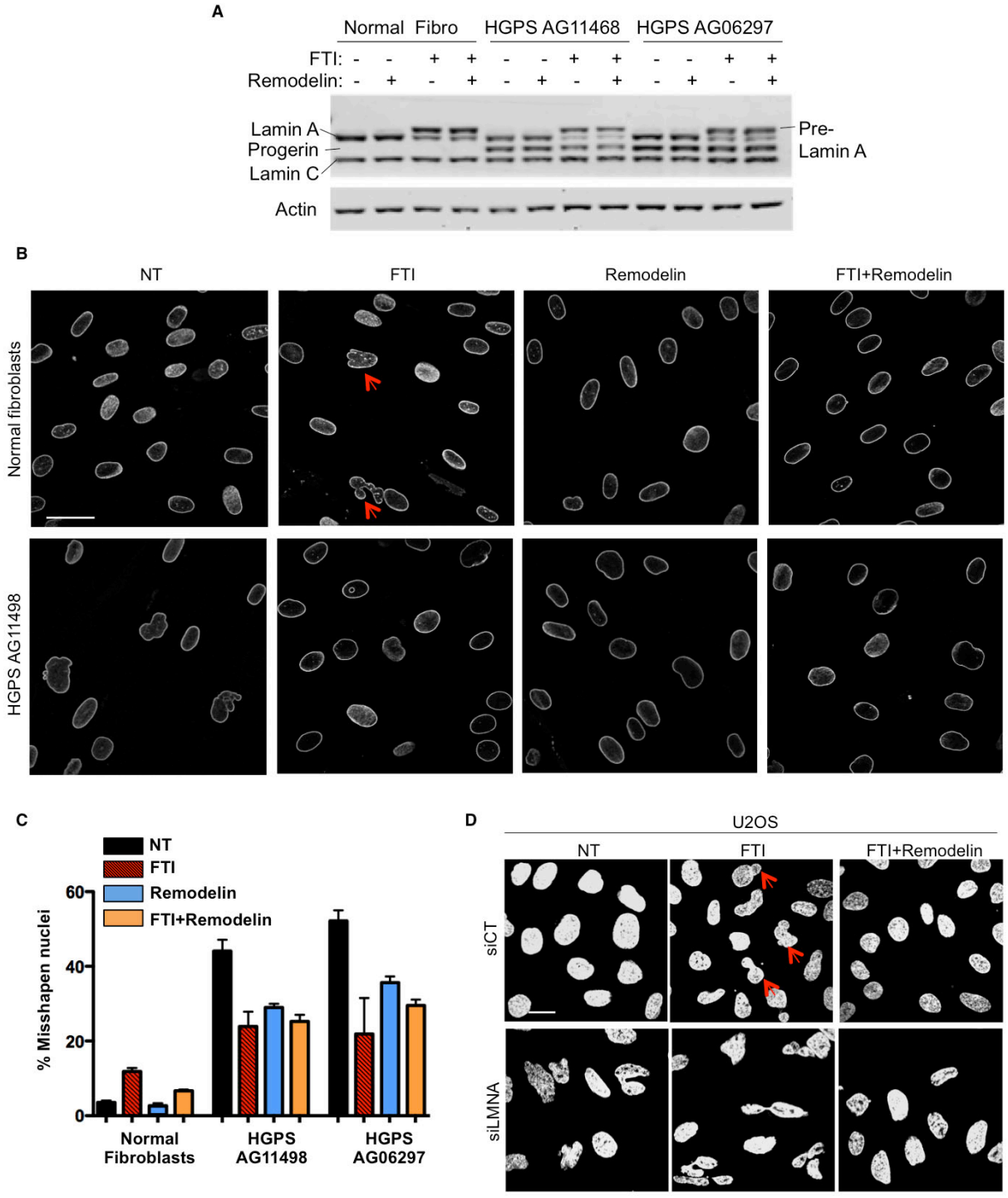

Fig. S8: Remodelin prevents FTI induced nuclear shape defects in non-progeric cells. A) Analysis of Lamin A/C processing after Remodelin or FTI treatment, showing that Remodelin is not a FTI. **B)** Representative pictures of Lamin A/C IF staining after the indicated treatments. Arrows indicate FTI induced misshapen nuclei in normal fibroblasts. Scale bar: 50 µm. **C)** Quantification of misshapen nuclei with the indicated cell lines and inhibitor treatments (means of three independent experiments ± s.e.m.

n>178). **D)** Representative pictures of DAPI staining showing effects of FTI and Remodelin on nuclear shape of U2OS cells. Scale bars: 20 μm.

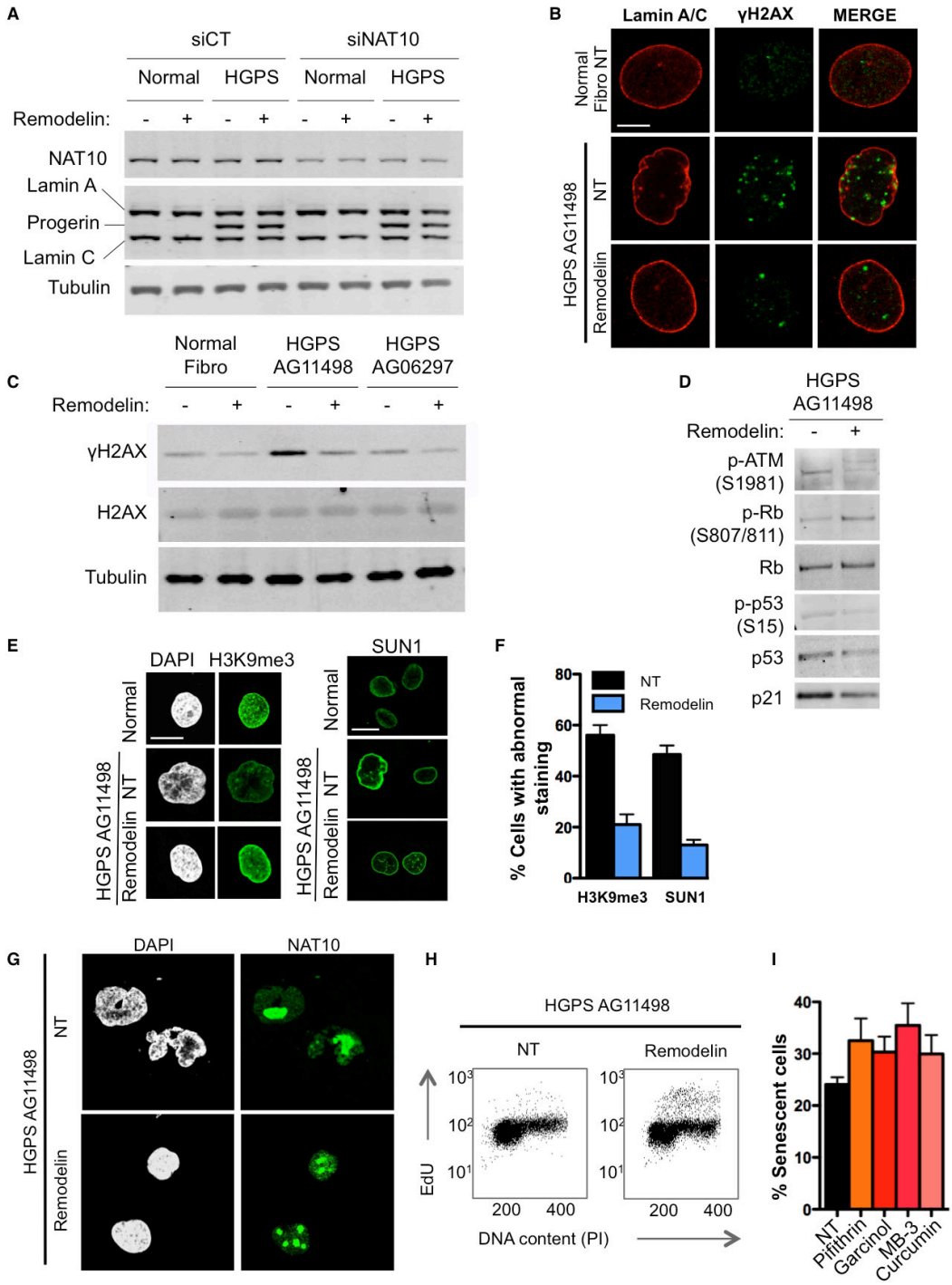

Fig. S9: Remodelin improves global cellular fitness of HGPS cells. A) NAT10 depletion in normal fibroblasts and HGPS AG11498 cells observed by western blotting, and showing that siNAT10 has no effect on Lamin A/C expression and processing. **B)** IF images showing nuclear shape improvement and decreased numbers of γH2AX foci in HGPS cells upon Remodelin treatment. Scale bars: 10 µm. **C)** Western Blotting analysis showing that Remodelin decreases γH2AX levels in both HGPS cell lines tested. **D)**

Western blotting analysis showing the effect of Remodelin on the p53 and DNA damage signalling pathways in HGPS AG11498 cells. **E)** Representative IF images of H3K9me3 or SUN1 patterns quantified in **F)**. Scale bars: 20 μm. **G)** IF staining showing more intense and homogenous DAPI staining, as well as reorganization of nucleolus architecture as observed by NAT10 staining upon Remodelin treatment. Scale bars: 10 μm. **H)** Flow cytometry analysis after 2 hours of EdU incorporation in HGPS cells upon Remodelin treatment showing enhancement of DNA replication rate. **I)** Quantification of senescence-associated β-galactosidase positive cells after treatment with p53 inhibitor (Pifithrin) or with the indicated KAT inhibitors, showing that none of these compounds decrease the senescence in HGPS AG11498.

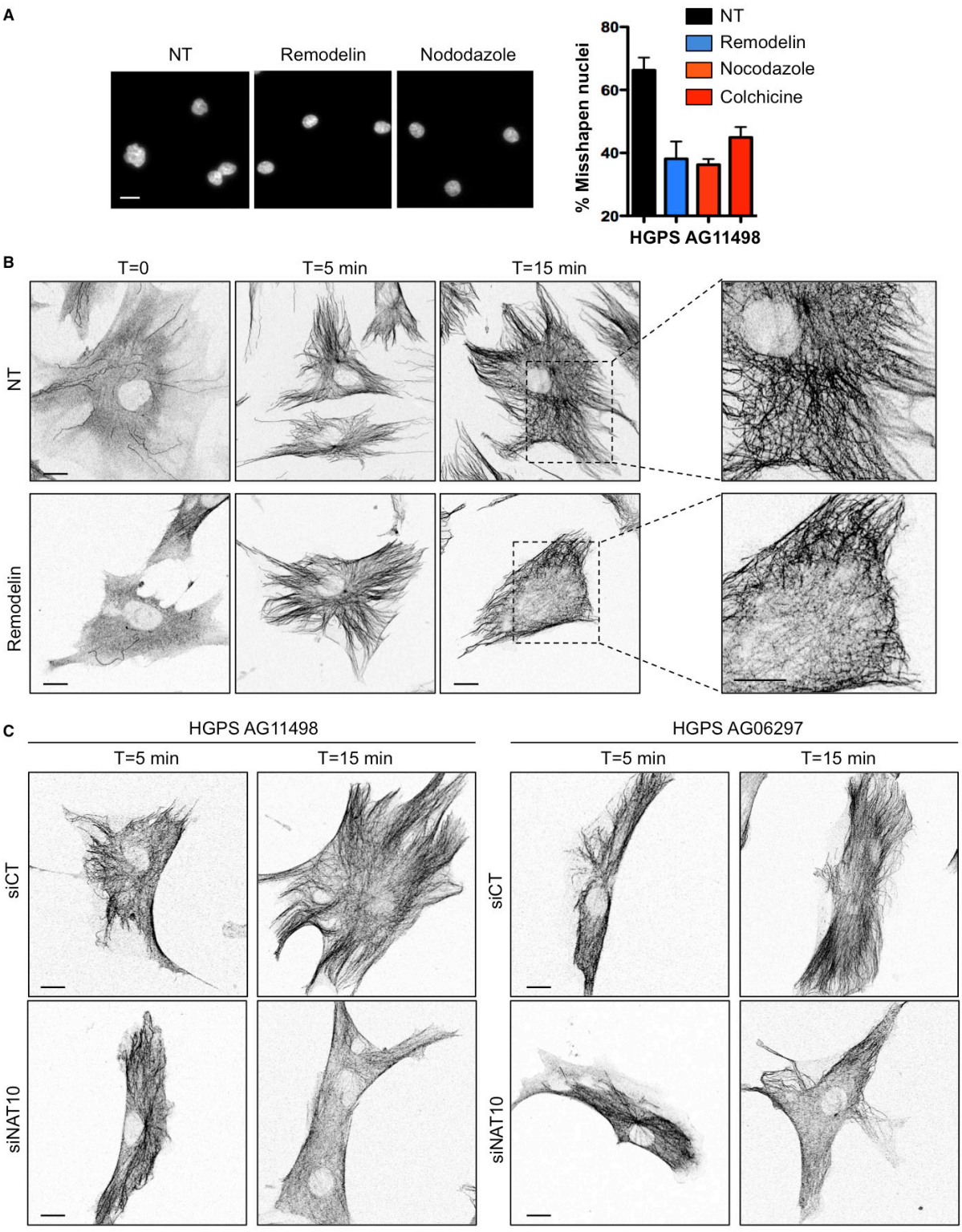

Fig. S10: Remodelin targets the microtubule network in HGPS cells to improve nuclear shape. A) Nuclear shape visualisation and quantification after treating cells with microtubule-disrupting agents. **B)** Microtubule regrowth assay in HGPS AG11498 cells

treated with Remodelin. α-tubulin inverted IF staining shows normal microtubule depolymerisation (T=0) and nucleation phase (T=5 min) but defects in the microtubule anchorage (T=15 min) upon Remodelin treatment. **C) ** Microtubule regrowth assay as in **B)** showing defects in the microtubule anchorage (T=15 min) upon NAT10 depletion (siNAT10) in the indicated HGPS cell lines and compared to cells transfected with control siRNA (siCT). Scale bars: 20 μm.

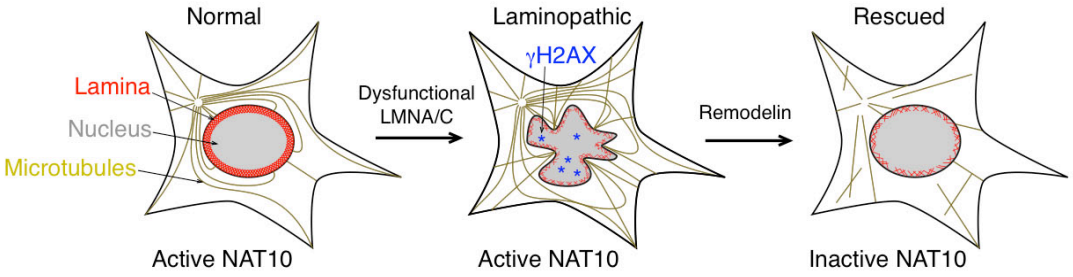

Fig. S11: Model of nuclear shape rescue by Remodelin. Laminopathic cells have enlarged, misshapen nuclei associated with disorganized chromatin structure. Upon Remodelin treatment, NAT10 acetyltransferase activity is inhibited, leading to disruption of microtubule anchorage at the centrosome and release of microtubule forces on the nuclear envelope. This release of mechanical stress on the nucleus contributes to nuclear shape rescue and global improvement of cell fitness and chromatin organization. Additional nuclear function of NAT10 might also contribute to chromatin reorganization, decreased DNA damage and decreased senescence.

Movie S1: Live imaging of nuclear shape rescue in siLMNA cells. U2OS stably expressing GFP-H2B were transfected by siLMNA and treated with Remodelin. Pictures were acquired every 15 min over 12 h.